

# The astrophysical $S$ –factor and reaction rate for $^{15}\text{N}(p,\gamma)^{16}\text{O}$ within the modified potential cluster model

S. B. Dubovichenko,<sup>1</sup> A. S. Tkachenko,<sup>1</sup> R. Ya. Kezerashvili,<sup>2,3</sup> N. A. Burkova,<sup>4</sup> and B. M. Yeleusheva<sup>1,4</sup>

<sup>1</sup>*Fesenkov Astrophysical Institute, 050020 Almaty, Kazakhstan*

<sup>2</sup>*New York City College of Technology, City University of New York, Brooklyn, 11201 New York, USA*

<sup>3</sup>*Graduate School and University Center, City University of New York, 10016 New York, USA*

<sup>4</sup>*al-Farabi Kazakh National University, 050040 Almaty, Kazakhstan*

We study a radiative  $p^{15}\text{N}$  capture on the ground state of  $^{16}\text{O}$  at stellar energies within the framework of a modified potential cluster model (MPCM) with forbidden states, including low-lying resonances. The investigation of the  $^{15}\text{N}(p,\gamma)^{16}\text{O}$  reaction includes the consideration of  $^3S_1$  resonances due to  $E1$  transitions and the contribution of  $^3P_1$  scattering wave in  $p + ^{15}\text{N}$  channel due to  $^3P_1 \rightarrow ^3P_0$   $M1$  transition. We calculated the astrophysical low-energy  $S$ –factor, and extrapolated  $S(0)$  turned out to be within  $34.7 - 40.4$  keV·b. The important role of the asymptotic constant (AC) for the  $^{15}\text{N}(p,\gamma)^{16}\text{O}$  process with interfering  $^3S_1(312)$  and  $^3S_1(962)$  resonances is elucidated. A comparison of our calculation for  $S$ –factor with existing experimental and theoretical data is addressed, and a reasonable agreement is found.

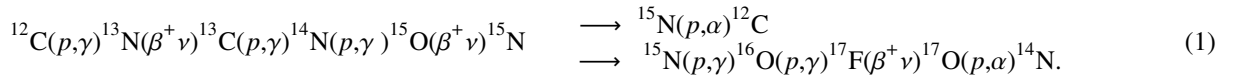
The reaction rate is calculated and compared with the existing rates. It has negligible dependence on the variation of AC, but shows a strong impact of the interference of  $^3S_1(312)$  and  $^3S_1(962)$  resonances, especially at temperatures, referring to the CNO Gamow windows. We estimate the contribution of cascade transitions to the reaction rate based on the exclusive experimental data by *Imbriani, et al. 2012*. The reaction rate enhancement due to the cascade transitions is observed from  $T_9 > 0.3$  and reaches the maximum factor  $\sim 1.3$  at  $T_9 = 1.3$ .

We present the Gamow energy window and a comparison of rates for radiative proton capture reactions  $^{12}\text{N}(p,\gamma)^{13}\text{O}$ ,  $^{13}\text{N}(p,\gamma)^{14}\text{O}$ ,  $^{14}\text{N}(p,\gamma)^{15}\text{O}$ , and  $^{15}\text{N}(p,\gamma)^{16}\text{O}$  obtained in the framework of the MPCM and give temperature windows, prevalence, and significance of each process.

Keywords: low and astrophysical energies,  $p^{15}\text{N}$  system, thermonuclear reaction rate, potential cluster model, CNO-cycle

## I. INTRODUCTION

Stellar burning depend on the star’s initial mass and can proceed either through the  $p$ – $p$  chain or through the Carbon–Nitrogen–Oxygen (CNO) cycle, fusing hydrogen to helium through a chain fusion processes, – sequence of thermonuclear reactions that provides most of the energy radiated by the hot stars [1–3]. Unlike the  $p$  –  $p$  chain, the CNO cycle is a catalytic one, that converts 4 protons into one helium nucleus but does so via reactions on the pre-existent seed isotopes of carbon, nitrogen, and oxygen nuclei. The carbon, nitrogen, and oxygen isotopes act just as catalysts in the CNO cycle. The CNO bi-cycle involves the following chains of nuclear reactions:



Therefore, the CNO bi-cycle produces three electron neutrinos from  $\beta^+$  decay of  $^{13}\text{N}$ ,  $^{15}\text{O}$ , and  $^{17}\text{F}$  and is also referred to as the “cold” CNO cycle [4]. The CN cycle contains no stable  $^{13}\text{N}$  and  $^{15}\text{O}$  isotopes, that decay to the stable isotopes  $^{13}\text{C}$  and  $^{15}\text{N}$ , respectively. The catalytic nuclei are lost from the process via the leak reaction  $^{15}\text{N}(p,\gamma)^{16}\text{O}$  and the subsequent reactions in (1) restore the catalytic material, generating  $^{16}\text{O}$  and heavier isotopes leading to the accumulation of the  $^4\text{He}$  and  $^{14}\text{N}$  nuclei. This second branch produces  $^{17}\text{F}$ , which  $\beta^+$  decay with the emission of the 1.74 MeV electron neutrinos. Thus, the  $^{15}\text{N}(p,\gamma)^{16}\text{O}$  process represents a branching reaction linking the alternative NO channel of the CNO cycle that produces the stable oxygen isotopes [5]. Therefore, in the CNO cycle, the proton capture reaction on  $^{15}\text{N}$  allows two possible channels: the branch of the cycle  $^{15}\text{N}(p,^4\text{He})^{12}\text{C}$  and the branch of the cycle  $^{15}\text{N}(p,\gamma)^{16}\text{O}$ , reactions and they intersect at the  $^{15}\text{N}$  nucleus.

The rate of the CN with respect to the NO cycle depends on the branching ratio of the  $^{15}\text{N}(p,\gamma)^{16}\text{O}$  and  $^{15}\text{N}(p,\alpha)^{12}\text{C}$  reaction cross sections. The probability for the  $^{15}\text{N}(p,\gamma)^{16}\text{O}$  process to occur is about one for every thousand of the second [6], thus the contribution to the overall nuclear energy production is negligible, while the consequences on the nucleosynthesis are critical [7]. Therefore, in the case of an active NO cycle, the correct evaluation of the  $^{15}\text{N}(p,\gamma)^{16}\text{O}$  reaction is crucial to properly predict the abundances of all the stable  $^{16}\text{O}$ ,  $^{17}\text{O}$ , and  $^{18}\text{O}$  isotopes and their relative ratios [8–10]. The reaction rates ratio determines on how much nucleosynthesis of  $^{16}\text{O}$ ,  $^{17}\text{O}$ , and  $^{18}\text{O}$  takes place during CNO burning [8].

Since the first experimental study of  $^{15}\text{N}(p,\gamma)^{16}\text{O}$  reaction in 1952 [11] experimental data [6, 12–17] for total cross sections of the radiative  $p^{15}\text{N}$  capture in the energy region from 80 keV to 2.5 MeV were collected [18, 19]. Analysis of existing

experimental measurements of the low-energy  $^{15}\text{N}(p,\gamma)^{16}\text{O}$  reaction shows that cross section data differ substantially at lower energies.

In the past, a variety of theoretical approaches from potential cluster models to multilevel  $R$ -matrix formalisms [5, 16, 20–23] were used to describe the  $^{15}\text{N}(p,\gamma)^{16}\text{O}$  reaction cross section at the stellar energies and astrophysical  $S$ -factor that is the main characteristic of this process at low energies. In the framework of the selective resonant tunneling model [24]  $^{15}\text{N}(p,\gamma)^{16}\text{O}$  cross section and  $S$ -factor have been studied [25]. Most recently, the astrophysical  $S$ -factor for the radiative proton capture process on the  $^{15}\text{N}$  nucleus at stellar energies are studied within the framework of the cluster effective field theory [26, 27]. The authors perform the single channel calculations where only the contribution of the first resonance into a cross section was considered [26] and then reported the results by including two low-energy resonances [27].

In this paper we are continuing the study of the reactions of radiative capture of protons on light atomic nuclei [28, 29] and consider the radiative proton capture on  $^{15}\text{N}$  at astrophysical energies in the framework of a modified potential cluster model (MPCM). Within the MPCM over thirty reactions of radiative capture of protons, neutrons and other charged particles on light atomic nuclei were considered and results are summarized in [30, 31]. References [28, 29] provide the basic theoretical framework of the MPCM approach for the description of a charged-particle-induced radiative capture reactions. Calculation methods based on the MPCM of light nuclei with forbidden states (FS) are used [32]. The presence of allowed states (AS) and FS are determined based on the classification of the orbital states of clusters according to Young diagrams [33]. Our analysis is data driven: the potentials of intercluster interactions for scattering processes are constructed based on the reproduction of elastic scattering phase shifts, taking into account their resonance behavior or the spectra of the levels of the final nucleus. For the bound states (BS) or ground state (GS) of nuclei in cluster channels, intercluster potentials are built based on a description of the binding energy, asymptotic normalization coefficient (ANC) and mean square radius [28, 29, 31].

The modified model includes a classification of orbital states according to Young's diagrams. This classification leads to the concept of "forbidden states" in interaction potentials. In particular, for the GS of the  $p^{15}\text{N}$  system, the potential has a deeply bound state, which is the FS, and the second bound state is the GS of the  $^{16}\text{O}$  nucleus in this channel. The concept of forbidden states makes it possible to effectively take into account the Pauli principle for multinucleon systems when solving problems in cluster models for a single-channel approximation. The current study is based on the detailed classification of orbital states in  $p + ^{15}\text{N}$  channel by Young's diagrams we performed early in Ref. [22].

In this work we study a radiative  $p^{15}\text{N}$  capture on the ground state of  $^{16}\text{O}$  within the framework the MPCM. For the first time the contribution of  $^3P_1$  scattering wave in  $p + ^{15}\text{N}$  channel due to  $^3P_1 \rightarrow ^3P_0 M1$  transition is considered. Our approach allows to analyze the explicit contribution of each transition into the  $S$ -factor and show the origin of the interference for  $E1$  transitions.

This paper is organized as follows. Section II presents a structure of resonance states and construction of interaction potentials based on the scattering phase shifts, mean square radius, asymptotic constant and bound states or ground state of  $^{16}\text{O}$  nucleus. Results of calculations of the astrophysical  $S$ -factor and reaction rate for the proton radiative capture on  $^{15}\text{N}$  are presented in Secs. III and IV, respectively. In the same sections we discuss a comparison of our calculation for  $S$ -factor and reaction rate with existing experimental and theoretical data. Conclusions follow in Sec. V.

## II. INTERACTION POTENTIALS AND STRUCTURE OF RESONANCE STATES

The  $E1$  transitions from resonant  $^3S_1$ -scattering states are the main contributions to the total cross section of the radiative proton capture on  $^{15}\text{N}$  to the ground state of  $^{16}\text{O}$  [5]. In the channel of  $p + ^{15}\text{N}$  in continuum there are two  $^3S_1$  resonances:

1. The first resonance appears at an energy of 335(4) keV with a width of 110(4) keV in the laboratory frame and has a quantum numbers  $J^\pi, T = 1^-, 0$  (see Table 16.22 in [34]). This resonance is due to the triplet  $^3S_1$  scattering state and leads to  $E1$  transition to the GS. In the center-of-mass (c.m.) frame this resonance is at an energy of 312(2) keV with a width of 91(6) keV and corresponds to the resonant state of the  $^{16}\text{O}$  at an excitation energy of  $E_x = 12.440(2)$  MeV (see Table 16.13 in [34]). However, in the new database [35], for this resonance, the excitation energy of  $E_x = 12.445(2)$  MeV and the width of  $\Gamma = 101(10)$  keV in the c.m. are reported.

2. The second resonance is at an energy of 1028(10) keV with a width of 140(10) keV in laboratory frame and has a quantum numbers  $J^\pi = 1^-$  and  $T = 1$  [34]. This resonance is also due to the triplet  $^3S_1$  scattering and leads to  $E1$  transition to the GS of  $^{16}\text{O}$ . In the c.m. the resonance emerges at an energy of 962(2) keV with a width of  $\Gamma = 139(2)$  keV and corresponds to the excitation energy of  $E_x = 13.090(2)$  MeV of  $^{16}\text{O}$  in a new database [35]. In the database [34] for this resonance, the excitation energy of  $E_x = 13.090(8)$  MeV and width of  $\Gamma = 130(5)$  keV in the c.m. are reported.

The compilation of experimental data on the  $^3S_1$  resonances is presented in Table 1.

In databases [34, 35] are reported the other resonances as well. The third resonance has an energy of 1640(3) keV with a width of 68(3) keV in the laboratory frame and quantum numbers  $J^\pi, T = 1^+, 0$ . This resonance can be due to the triplet  $^3P_1$  scattering and leads to  $M1$  transition to the GS. The resonance is at an energy of 1536(3) keV with a width of 64(3) keV in the c.m. that

TABLE 1. Data on the  ${}^3S_1$  resonance states in  $p + {}^{15}\text{N}$  channel.  $E_x$  is the excitation energy,  $E_{\text{res}}$  and  $\Gamma_{\text{res}}$  are the experimental resonance energy and the width, respectively.  $E_{\text{theory}}$  and  $\Gamma_{\text{theory}}$  are the resonance energy and the width, respectively, obtained in the present calculations.

${}^{2S+1}L_J$	$E_x$ , MeV	$E_{\text{res}}$ , keV	$\Gamma_{\text{res}}$ , keV	$E_{\text{theory}}$ , keV	$\Gamma_{\text{theory}}$ , keV
${}^3S_1(312)$	12.440(2) [34]	312(2) [34]	91(6) [34]	312	125 – 141
	12.445(2)[35]	317(2) [35]	101.5(10) [35]		
${}^3S_1(962)$	13.090(8) [34]	962(8) [34]	130(5) [34]	962	131
	13.090(2) [35]	962(2) [35]	139(2) [35]		

corresponds to the excitation energy 13.664(3) MeV of the  ${}^{16}\text{O}$  [34] and in Ref. [35] the excitation energy of 13.665(3) MeV and the width of 72(6) keV in the c.m. are reported. However, this resonance was observed only in measurements [13], and in the later measurements [16, 17] the resonance is absent. Therefore, we will not consider it in our calculations. The next resonance is excited at the energy of 16.20(90) MeV ( $J^\pi, T = 1^-, 0$ ) has a larger width of 580(60) keV in the c.m. and its contribution to the reaction rate will be small. In addition, in the spectra of  ${}^{16}\text{O}$  [34], another resonance is observed at an excitation energy of 16.209(2) MeV ( $J^\pi, T = 1^+, 1$ ) with a width of 19(3) keV in the c.m. However, the resonance energy is too large and its width too small to make a noticeable contribution to the reaction rates.

The cascade transitions via two very narrow  $2^-$  resonances as well as the  $0^-$  and  $3^-$  resonances in the  $0.40 \leq E_R \leq 1.14$  MeV range [17, 36, 37] are considered for the reaction rate calculations. These cascading transitions are included in the NACRE II [19] reaction rate calculations and appear at high  $T_9$ . There are two  $2^-$  resonances [17], at the excitation energies of 12.53 MeV and 12.9686 MeV with the widths of 97(10) eV and 1.34(4) keV [35], respectively. When one considers transitions to the ground state with  $0^+$ , only  $M2$  transitions are possible here, which have a very small cross section, and we do not consider them. In addition, due to such small widths, their contribution to the reaction rate will be very small. The measurement of the excitation functions of the three dominant cascade transitions allows one to estimate of the contributions from these transitions. In Ref. [5] capture processes to the GS and three excited states  $E_x = 6.049$  MeV, 6.130 and 7.117 MeV are considered, that gives  $S(0) = 41(3)$  keV·b in total while 40(3) keV·b for the GS. It is shown that the  $1^-$  and two  $2^+$  resonances do not affect the value of the  $S$ -factor, two  $3^-$  resonances at  $E_x = 13.142$  MeV and 13.265 MeV decay into the GS due to the  $E3$  transition and their contribution is negligible [5].

On the background of strong  $E1$  transitions the next one in the long-wave expansion of the electromagnetic Hamiltonian is magnetic dipole  $M1$  transition [38]. In the case of  ${}^{15}\text{N}(p, \gamma_0){}^{16}\text{O}$ ,  $M1$  transition is allowed by selection rules. It occurs as a direct capture from the non-resonance scattering wave  ${}^3P_1$  to the  ${}^{16}\text{O}$   ${}^3P_0$  state. The intensity of the  $M1$  partial transition depends on the distorted  ${}^3P_1$  wave only and is related to the corresponding interaction potential. Our estimations of the  $M1$  partial cross section in plane-wave approximation shows near order of magnitude suppression. The inclusion of the  $p$ -wave interaction in  $p+{}^{15}\text{N}$  channel enhances the  $M1$  transition. The interaction potential could be constructed based on an elastic  ${}^{15}\text{N}(p, p){}^{15}\text{N}$  scattering to describe the  ${}^3P_1$  phase shift. The phase shifts should satisfy the following conditions: i. at  $E = 0$  the  $\delta_{p, P_1} = 180^\circ$  according to the generalized Levinson theorem [32]; ii. fit the existing  $p$ -wave  ${}^{15}\text{N}(p, p){}^{15}\text{N}$  scattering data. iii. have a non-resonance behaviour. Below we found potential parameters that provides a reasonable phase shifts. Therefore, in calculations we are considering only the above two  ${}^3S_1$  resonance transitions and non-resonance  ${}^3P_1$  scattering for the  $M1$  transition to the  ${}^{16}\text{O}$  GS.

We should distinguish  $M1$  capture from the non-resonance  ${}^3P_1$  scattering wave to the  ${}^{16}\text{O}$   ${}^3P_0$  state and  $M1$  de-excitation of  $1^+$  level at 13.665 MeV to the ground state. As pointed by *deBoer et al.* [5]: “The  $1^+$  level at  $E_x = 13.66$  MeV could decay by  $M1$  de-excitation to the ground state but no evidence for this is observed (contrary to Ref. [13]).” As mentioned above we are not considering the contribution of  $M1$  de-excitation ( $1^+$  level at 13.665 MeV) to the  $S(E)$ .

For calculations of the total radiative capture cross sections, the nuclear part of the  $p+{}^{15}\text{N}$  interaction potential is contracted using Gaussian form [28, 29, 31]:

$$V(r, JLS, \{f\}) = -V_0(JLS, \{f\}) \exp(-\alpha(JLS, \{f\})r^2). \quad (2)$$

The parameters  $\alpha$  and  $V_0$  in Eq. (2) are the interaction range and the strength of the potential, respectively.

The strength and the interaction range of the potential (2) depend on the total and angular momenta, the spin,  $JLS$ , and Young diagrams  $\{f\}$  [30, 31]. For description of the  ${}^3S_1$  scattering states we use the corresponding experimental energies and widths from Table 1. Coulomb potential is chosen as point-like interaction potential.

Construction of the potentials that give the energies and widths of  ${}^3S_1(312)$  and  ${}^3S_1(962)$  resonances reported in the literature is a challenging task. One has to find the optimal parameters of the potentials for the description of  $E1$  transitions that lead to the fitting of the experimental resonance energies and the widths of both interfering resonances. For the  ${}^3S_1(962)$  resonance the found optimal parameters of the interaction potential that allow to reproduce the resonance energy  $E_{\text{res}} = 962(1)$  keV and width

TABLE 2. Parameters of interaction potentials  $V_0$  and  $\alpha$  for the GS and continuum states. The  $C_W$  is a dimensionless constant that corresponds to the range of the experimental ANC  $12.88 - 14.76 \text{ fm}^{-1/2}$  [21, 23]. The theoretical widths,  $\Gamma_{\text{theory}}$ , for the resonance  ${}^3S_1(312)$  and  ${}^3S_1(962)$  are calculated using the corresponding parameters of the potentials.  $V_0$  and  $\Gamma_{\text{theory}}$  are given in MeV and keV, respectively,  $\alpha$  in  $\text{fm}^{-2}$ , and ANC in  $\text{fm}^{-1/2}$ .

Set	${}^3P_0$ , GS				${}^3S_1(312)$ , E1			${}^3S_1(962)$ , E1			${}^3P_1$ , M1	
	$V_0$	$\alpha$	ANC	$C_W$	$V_0$	$\alpha$	$\Gamma_{\text{theory}}$	$V_0$	$\alpha$	$\Gamma_{\text{theory}}$	$V_0$	$\alpha$
I	976.85193	1.1	14.49	2.05	1.0193	0.0028	141					
II	1057.9947	1.2	13.71	1.94	1.0552	0.0029	131	105.0675	1.0	131	14.4	0.025
III	1179.3299	1.35	12.85	1.8	1.0902	0.003	125					

$\Gamma_{\text{res}} = 131 \text{ keV}$  are reported in Table 2. The situation is more complicated with the  ${}^3S_1(312)$  resonance. While it is possible to reproduce rather accurately the position and the width of the  ${}^3S_1(312)$  resonance, the consideration of the interference of  ${}^3S_1$  resonances gives different sets of optimal parameters for the potential. We found three sets I – III of the optimal values for  $V_0$  and  $\alpha$  parameters reproducing exactly the energy of the first resonance  $E_{\text{theory}} = 312(1) \text{ keV}$ , but the width  $\Gamma_{\text{theory}}$  varies in the range of  $125 - 141 \text{ keV}$ .

The dependence of the elastic  $p^{15}\text{N}$  scattering phase shifts for the E1 transitions on the energy is shown in Fig. 1a. The result of the calculation of the  ${}^3S_1$  phase shifts with the parameters for the S scattering potential without FS from Table 2 leads to the value of  $90^\circ(1)$  at the energies  $312(1)$  and  $962(1) \text{ keV}$ , respectively. Our calculations of the phase shifts for the  ${}^3S_1(312)$  resonance with the parameter sets I - III show very close energy dependence in the entire energy range up to  $5 \text{ MeV}$  at a fixed resonance position.

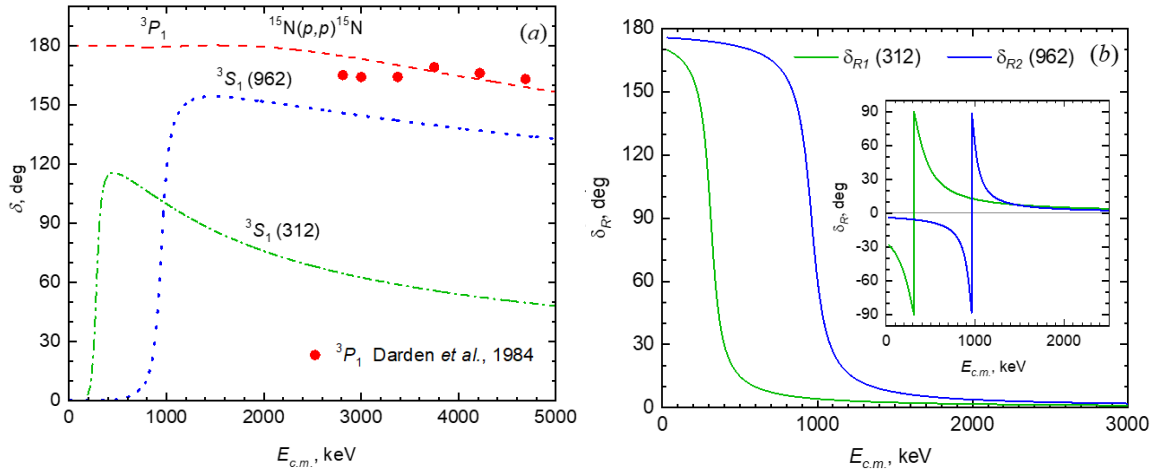


FIG. 1. (Color online) The dependence of the elastic  $p^{15}\text{N}$  scattering phase shifts on the energy. (a) Calculations are performed by using the potentials with parameters from Table 2. The phase shifts for  ${}^3S_1(312)$  resonance is calculated using the set I and is shown by the dash-dotted curve. The phase shifts for  ${}^3S_1(962)$  resonance and  ${}^3P_1$  are presented by the dotted and dashed curves, respectively. The experimental data from Ref. [42]. (b) The energy dependence of the resonant phase shifts  $\delta_{R1}$  and  $\delta_{R2}$  calculated using the experimental resonance widths  $91 \text{ keV}$  and  $130 \text{ keV}$ , respectively. Reconstructed scattering resonant phase shifts  $\delta_{R1}$  and  $\delta_{R2}$  are calculated using Eq. (3) and taking into account the tangent function periodicity. The insert shows the result of calculation using Eq. (3).

In elastic  $p^{15}\text{N}$  scattering spectra at energies up to  $5 \text{ MeV}$ , there are no resonance levels with  $J^\pi = 0^+, 1^+, 2$  except for the mentioned above, and widths greater than  $10 \text{ keV}$  [34]. Therefore, for potentials of non-resonance  ${}^3P$ -waves with one bound FS parameters can be determined based on the assumption that in the energy region under consideration their phase shifts are practically zero or have a gradually declining character [29]. For such potential the optimal parameters are:  $V_p = 14.4 \text{ MeV}$ ,  $\alpha_p = 0.025 \text{ fm}^{-2}$ . The result of the calculation of  $P$ -phase shifts with such potential at an energy of up to  $5 \text{ MeV}$  is shown in Fig. 1a. To determine the values of phase shifts at zero energy, we use the generalized Levinson theorem [32], so the phase shifts of the potential with one bound FS should begin from  $180^\circ$ . In the energy region  $E_{c.m.} < 5 \text{ MeV}$  the  ${}^3P_1$  phase shift has gradual energy dependence and it is almost constant up to  $E_{c.m.} \approx 2.2 \text{ MeV}$ .

It is interesting to compare experimentally determined phase shifts with our calculations. While in Ref. [39] the elastic

scattering of protons from  $^{15}\text{N}$  was studied and authors measured the excitation functions of  $^{15}\text{N}(p,p)^{15}\text{N}$  over the proton energy range from 0.6 to 1.8 MeV at some laboratory angles, there been no phase shifts reported. There has been no systematic experimentally determined phase shifts at the energies of the astrophysical interest. Absolute differential cross sections were measured for the reactions  $^{15}\text{N}(p,p)^{15}\text{N}$  [40] and spins and parities are discussed where resonances suggest the existence of excited states in  $^{16}\text{O}$ . In Ref. [41] authors carried out a phase-shift analysis of cross section for the energy interval 8–15 MeV. Angular distributions of cross section and analyzing power for elastic scattering of protons from  $^{15}\text{N}$  have been measured for the energy interval 2.7–7 MeV [42], and the authors gave a phase-shift analysis of data. Results of our calculations for the  $^3P_1$  phase shift along with the experimental data [42] are presented in Fig. 1a.

The main assumption in all previous studies of the reaction  $^{15}\text{N}(p,\gamma)^{16}\text{O}$  was that a direct and resonant radiative capture cross sections and their interferences contribute to the total cross section. The direct radiative capture process is considered assuming a potential peripheral radiative capture for a hard sphere scattering [13, 43–46]. However, in general, phase shifts are extracted from experimental data analysis without the separation on the potential and resonant terms [47, 48]. We follow this Ansatz. Consequently, the  $E1$  transition amplitudes are constructed based on a single radial scattering wave function resembling continuous, both smooth and resonance energy dependence. Both  $^3S_1$  phase shifts obtained with these scattering wave functions depend on the energy as shown in Fig. 1a. Therefore, we have only the interference between two partial  $E1$  matrix elements in contrast to all previous considerations.

The resonant phase shift is given by the usual expression [13, 48]

$$\delta_R = \tan^{-1} \frac{\Gamma}{2(E - E_{res})}, \quad (3)$$

where  $\Gamma$  is the width of a resonance. In Fig. 1b the energy dependence of the resonant  $\delta_{R1}$  and  $\delta_{R2}$  phase shifts for the resonance width 312 keV and 962 keV is presented, respectively. The comparison of the phase shifts for the  $E1$  transitions via the  $^3S_1(312)$  and  $^3S_1(962)$  resonances with the resonant phase shifts  $\delta_{R1}$  and  $\delta_{R2}$  shows their different energy dependence.

We construct the potential for  $^{16}\text{O}$  in GS with  $J^\pi, T = 0^+, 0$  in  $p^{15}\text{N}$ -channel based on the following characteristics: the binding energy of 12.1276 MeV, the experimental values of 2.710(15) fm and 2.612(9) fm [34] for the root mean square radii of  $^{16}\text{O}$  and  $^{15}\text{N}$  of [49], respectively, and a charge and matter radius of a proton 0.8414 fm [50]. The potential also should reproduce the AC. The corresponding potential includes the FS and refers to the  $^3P_0$  state.

Usually for a proton radiative capture reaction of astrophysical interest one assumes that it is peripheral, occurring at the surface of the nucleus. If the nuclear process is purely peripheral, then the final bound-state wave function can be replaced by its asymptotic form, so the capture occurs through the tail of the nuclear overlap function in the corresponding two-body channel. The shape of this tail is determined by the Coulomb interaction and is proportional to the asymptotic normalization coefficient. The role of the ANC in nuclear astrophysics was first discussed by Mukhamedzhanov and Timofeyuk [51] and in Ref. [52]. These works paved the way for using the ANC approach as an indirect technique in nuclear astrophysics. See Refs. [45, 53–60] and citation herein and the most recent review [46].

We construct a potential with the FS  $^3P_0$  state using the experimental ANC given in Ref. [21] that relates to the asymptotics of radial wave function as  $\chi_L(R) = CW_{-\eta L+1/2}(2k_0R)$ . The dimensional constant  $C$  is linked with the ANC via the spectroscopic factor  $S_F$ . In our calculations we exploited the dimensionless constant [61]  $C_W$ , which is defined in [29] as  $C_W = C/\sqrt{2k_0}$ , where  $k_0$  is wave number related to the binding energy. In Ref. [21] the values 192(26) fm $^{-1}$  and 2.1 were reported for the ANC and spectroscopic factor, respectively. In Ref. [23] the dimensional ANC includes the antisymmetrization factor  $N$  into the radial

overlap function as it was clarified by authors in [59]. The factor  $N$  is defined as  $N = \binom{A}{x}^{1/2} = \sqrt{\frac{A!}{(A-x)!x!}}$ , where  $x$  and  $A$

are the atomic mass numbers of the constituent nucleus from  $x$  and  $A - x$  nucleons, respectively [62]. If  $x = 1$ , then  $N = \sqrt{A}$  and for the reaction  $^{15}\text{N}(p,\gamma_0)^{16}\text{O}$   $N = 4$ . Thus, using the experimental square of the ANC  $192 \pm 26 \text{ fm}^{-1}$  [21, 23], we obtained the interval for the dimensionless AC used in our calculations:  $C_W = 1.82 - 2.09$  that corresponds to the ANC of 12.88 – 14.76 fm $^{-1/2}$ . In the present calculations, we use for the proton mass  $m_p = 1.00727646677 \text{ amu}$  [50],  $^{15}\text{N}$  mass 15.000108 amu [63], and the constant  $\hbar^2/m_0 = 41.4686 \text{ MeV}\cdot\text{fm}^2$ , where  $m_0 = 931.494 \text{ MeV}$  is the atomic mass unit (amu).

The  $^{15}\text{N}(p,\gamma)^{16}\text{O}$  is the astrophysical radiative capture process, in which the role of the ANC is elucidated [46]. In Table 2 three sets of parameters for the  $^3P_0$  GS potential and AC  $C_W$  are listed. The asymptotic constant  $C_W$  is calculated over averaging at the interval 5 – 10 fm. Each set leads to the binding energy of 12.12760 MeV, the root mean square charge radius of 2.54 fm and the matter radius of 2.58 fm, but the sets of  $C_W$  lead to the different widths of the  $^3S_1(312)$  resonance.

Note, that there is one important benchmark for the choice of optimal sets for the parameters of interaction potentials for the first  $E1(312)$  resonance. There are the experimental values of the total cross section  $\sigma_{\text{exp}}(312) = 6.0 \pm 0.6 \mu\text{b}$  [6] and  $6.5 \pm 0.6 \mu\text{b}$  [16], which are in excellent agreement with earlier data  $6.3 \mu\text{b}$  [14] and  $6.5 \pm 0.7 \mu\text{b}$  [12]. Simultaneous variation of  $C_W$  for

the GS and parameters  $V_0$  and  $\alpha$  for the  ${}^3S_1(312)$  was implemented to keep the value of the cross section  $\sigma_{\text{theory}}(312) = 5.8 - 5.9 \mu\text{b}$  matching the experimental data. The result of this optimization is presented in Table 2 as sets I – III.

Table 2 summarizes the potential parameters used in the case where the MPCM works reasonably well for a radiative proton capture in the  ${}^{15}\text{N}(p,\gamma){}^{16}\text{O}$  reaction.

We sum up the procedure and choice of potential parameters as:

1. we construct the nucleon-nuclei potentials that give the channel binding energy with the requested accuracy  $10^{-5}$  MeV. There are a few such potentials;
2. the experimental ANC is used as a criterion for the choice of the potential that provides the required asymptotic behavior of the radial wave function at the fixed binding energy. Thus, the variety of wave function is constrained within the upper and lower limits for the ANC:  $12.88 - 14.76 \text{ fm}^{-1/2}$  for  ${}^{15}\text{N}(p,\gamma){}^{16}\text{O}$ ;
3. an additional test of the wave functions is a reproduction of the matter and charge radii with a precision of  $\sim 5\%$  and the  $\sigma_{\text{exp}}(312)$  cross section within experimental uncertainties;
4. for the continuous spectrum the parameters of the potential are fixed by the resonance energy and width above threshold. An additional source of the  $S$ -factor uncertainty relates to uncertainties of the resonance energy and width;
5. this procedure gives the model's uncertainty bands for the  $S$ -factor.

### III. ASTROPHYSICAL $S$ -FACTOR

The astrophysical  $S$ -factor is the main characteristic of any thermonuclear reaction at low energies. The present analysis focuses primarily on extrapolating the low-energy  $S$ -factor of the reaction  ${}^{15}\text{N}(p,\gamma){}^{16}\text{O}$  into the stellar energy range. Since the first experimental study of  ${}^{15}\text{N}(p,\gamma){}^{16}\text{O}$  reaction in 1960 [12], experimental data [6, 13, 16, 17, 19] for total cross sections of the radiative  $p$  ${}^{15}\text{N}$  capture in the energy region from 80 keV to 2.5 MeV have been collected. These experimental studies verified and confirmed that the radiative  $p$  ${}^{15}\text{N}$  capture is dominated by the first two interfering resonances at 312 keV and 962 keV with the quantum numbers  $J^\pi, T = 1^-, 0$  and  $J^\pi, T = 1^-, 1$ , respectively.

#### A. $E1$ transitions

The  $E1$  transitions are the main input parts of the radiative capture amplitude for  ${}^{15}\text{N}(p,\gamma){}^{16}\text{O}$  reaction. Therefore, it is required to determine the resonance capture cross sections for these transitions accurately to avoid one of the main sources of uncertainty. The radiative resonance capture to the bound states is reviewed in Ref. [46]. Following Ref. [29] after algebraic calculations using quantum numbers related to the  ${}^{15}\text{N}(p,\gamma){}^{16}\text{O}$  reaction, one can write the cross section for the radiative capture  $p$  ${}^{15}\text{N}$  to the ground state of  ${}^{16}\text{O}$  as

$$\sigma_{E1}(E_{\text{c.m.}}) = \frac{4\pi e^2}{9\hbar^2} \left(\frac{K}{k}\right)^3 \left(\frac{1}{m_p} - \frac{7}{m^{15}\text{N}}\right)^2 |I(k; E1)|^2. \quad (4)$$

In Eq. (4)  $\mu$  is the reduced mass of the proton and  ${}^{15}\text{N}$  nucleus,  $K = E_\gamma/\hbar c$  is the wave number of the emitted photon with energy  $E_\gamma$ ,  $k$  is relative motion wave number and

$$|I(k; E1)|^2 = \left| e^{-i\delta_{3S_1(312)}} I_1 + e^{-i\delta_{3S_1(962)}} I_2 \right|^2 = |I_1|^2 + |I_2|^2 + 2 \cos(\delta_{3S_1(312)} - \delta_{3S_1(962)}) I_1 I_2. \quad (5)$$

While constructing the radial matrix element in Eq. (4) squared by modulus, we pointed in Eq. (5) in explicit form the part of scattering  $S$ -matrix important for analyzing the interference effects (see, for example, Ref. [43]). Note that in the case of non-interfering amplitudes, phase-shift factor  $\exp(-i\delta_{LJ})$  converts to the unit in the final general expression for the total cross sections [29–31]. Below, we demonstrate that the interference term  $2 \cos(\delta_{3S_1(312)} - \delta_{3S_1(962)}) I_1 I_2$  plays an important role in the whole treated energy region, especially for the reaction rate at low temperatures (see insert in Fig. 4).

In Eq. (5) the overlapping integral between the initial  $\chi_i$  and final  $\chi_f$  states radial functions  $I(k) = \int_0^\infty \chi_i^* r \chi_f dr$  includes both the interior and asymptotic regions via the continuous functions. The specific behavior of the proton relative motion in the field of the  ${}^{15}\text{N}$  nucleus is taken into account via the nuclear interaction potential  $V(r)$ . That is according to the declared above Ansatz. Note that in the cluster model's single-channel approach, the asymptotic behavior of radial WF is actual for their proper normalizing [43].

As it is follows from Eq. (5) in the  $E1$  resonance  $\rightarrow$  ground state transitions the interference of  ${}^3S_1(312)$  and  ${}^3S_1(962)$  resonances gives the contribution into the cross section. The interference is determined by the difference of the  $\delta_{3S_1(312)}$  and

$\delta^3_{S_1(962)}$  phase shifts via the factor  $\cos(\delta^3_{S_1(312)} - \delta^3_{S_1(962)})$ . We depict the behavior of this factor as a function of energy in Fig. 2a using the phase shifts shown in Fig. 1. One can conclude that the contribution of the interfering term into the  $E1$  transitions cross section is very significant at the energies up to 2.5 MeV.

To illustrate the role of the factor  $\cos(\delta^3_{S_1(312)} - \delta^3_{S_1(962)})$ , we replace the  $\delta^3_{S_1(312)}$  and  $\delta^3_{S_1(962)}$  phase shifts by the resonant  $\delta_{R1}$  and  $\delta_{R2}$  (3). In this case, the factor  $\cos(\delta_{R1} - \delta_{R2})$  depends on the widths of the resonances. We calculate the energy dependence of the  $\cos(\delta_{R1} - \delta_{R2})$  by varying the width of the resonances from the experimental  $\Gamma_{R1} = 91$  keV and  $\Gamma_{R2} = 130$  keV [34] up to arbitrary values  $\Gamma_{R1} = 120$  keV and  $\Gamma_{R2} = 250$  keV (the upper and lower curves in Fig. 2, respectively). The results of the calculations are shown in Fig. 2 as a shaded area. We can conclude that the factor  $\cos(\delta_{R1} - \delta_{R2})$  is sensitive to the width of the resonances at the energy interval of about 400 – 800 keV and significantly increases the destructive interference term.

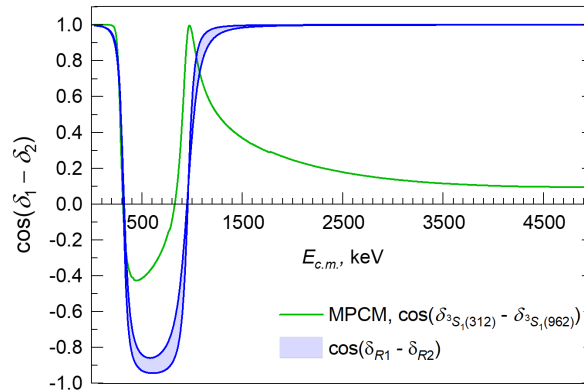


FIG. 2. The energy dependence of the factors  $\cos(\delta^3_{S_1(312)} - \delta^3_{S_1(962)})$  (green curve) and  $\cos(\delta_{R1} - \delta_{R2})$  (shaded area), respectively. The upper and lower curves of the shaded area are obtained with the  $\delta_{R1}$  and  $\delta_{R2}$  resonant phase shifts that are calculated for the experimental  $\Gamma_{R1} = 91$  keV,  $\Gamma_{R2} = 130$  keV and arbitrary  $\Gamma_{R1} = 120$  keV,  $\Gamma_{R2} = 250$  keV widths, respectively.

## B. Analysis of $S$ -factor

Results of calculations for the astrophysical  $S$ -factor based on the potential parameters given in Table 2 along with the compilation of experimental data [6, 13, 16, 17, 19] are presented in Fig. 3a. Notice that the contribution of  $2^+$  level at the excitation energy 12.97 MeV was considered in Ref. [5] using the  $R$ -matrix approach. The contribution of this transition to the GS is

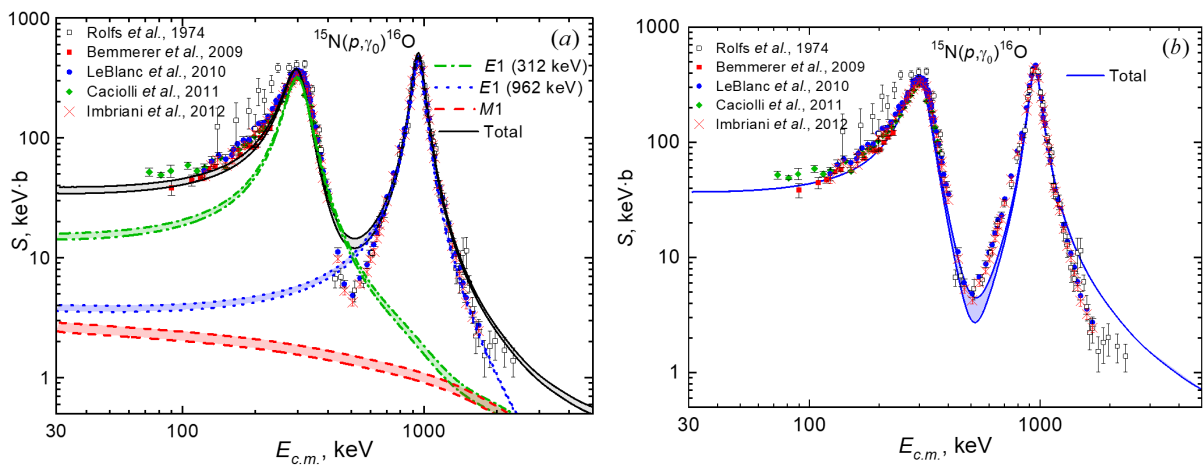


FIG. 3. (Color online) The astrophysical  $S$ -factor of radiative  $p^{15}\text{N}$  capture on the ground state of  $^{16}\text{O}$ . The shaded areas for the partial  $E1$ ,  $M1$ , and the total  $S$ -factors correspond to the calculations with parameters set I (upper curves) and III (lower curves) respectively, from Table 2. (b) The astrophysical  $S$ -factor is obtained with parameters set II, Table 2. The shaded area refers to the variation of the  $\cos(\delta_{R1} - \delta_{R2})$  factor for the interference term and corresponds to the shaded area in Fig. 2.

much smaller than non-resonance  $M1 \ ^3P_1 \longrightarrow \ ^3P_0$  transition. The contribution of the interference of  $\ ^3S_1(312)$  and  $\ ^3S_1(962)$  resonances leads to the significant increase of  $S$ -factor at the energies up to 300 keV. One can see the discrepancies between the experimental data and theoretical calculation at energies where the minimum of the  $S$ -factor is observed. This is related to the destructive interference of  $\ ^3S_1(312)$  and  $\ ^3S_1(962)$  resonances at this energy due to the factor  $\cos(\delta_{\ ^3S_1(312)} - \delta_{\ ^3S_1(962)})$ . This factor has a minimum at about 500 keV as it is depicted in Fig. 2. The minimum of the  $S$ -factor is reproduced precisely within the  $R$ -matrix approach [5] when the authors are considering the different reaction components' contributions in the fitting of the  $\ ^{15}\text{N}(p,\gamma)\ ^{16}\text{O}$  reaction data (see Fig. 49, [5]). Only by using the set of fitting parameters can be described the region of 0.5 MeV between resonances for the  $S$ -factor [5].

The shaded areas in Fig. 3a show the range of  $S(E)$  changes for different values of the AC. Thus, the values of transition amplitudes are governed by the AC. At an energy of 30–60 keV, the  $S$ -factor is practically constant and the corresponding value can be considered as the  $S$ -factor at zero energy. Thus, the theoretical calculation predicts very smooth behavior of  $S(E)$  at very low energies that converges to  $S(0) = 35.2(5)$  keV·b for  $C_W = 1.8$  (ANC of  $12.85 \text{ fm}^{-1/2}$ ). The increase of the AC leads to the increase of  $S(0)$ . The variation of the AC within the experimental uncertainties leads to the increase of the  $S$ -factor up to  $S(0) = 39.6(8)$  keV·b for  $C_W = 2.05$  (ANC of  $14.49 \text{ fm}^{-1/2}$ ). Therefore, depending on the value of the AC,  $S(0)$  varies in the range of 34.7 – 40.4 keV·b. Our predictions overlap with the value of the  $S(0)$  factor reported in Ref. [21]. Note that in Ref. [27] the value of 29.8(1.1) keV·b was obtained in the framework of the effective field theory. However, [27] describes the experimental  $S$ -factor with the resonances energies  $\approx 360$ –370 keV and widths  $\approx 250$ –350 keV for the first resonance and the resonances energies  $\approx 960$ –970 keV and widths  $\approx 155$ –160 keV for the second resonance, respectively, which are very far off from the experimental data.

Let us consider, as an example, a different calculation scenario for the  $S$ -factor to understand the discrepancies between the experimental data and theoretical calculation at energies where the  $S$ -factor has the minimum. The value and position of the minimum are determined by the destructive interference of  $\ ^3S_1(312)$  and  $\ ^3S_1(962)$  resonances. We calculate  $S$ -factor using Eq. (5) and the parameters set II from Table 2, but replace the factor  $\cos(\delta_{\ ^3S_1(312)} - \delta_{\ ^3S_1(962)})$  by  $\cos(\delta_{R1} - \delta_{R2})$ . The factor  $\cos(\delta_{R1} - \delta_{R2})$  is considered using the same parameters for the widths as shown in Fig. 2. The result of contributions of all transitions to the  $S(E)$  is shown by the shaded area in Fig. 3b. Thus, we demonstrate that by varying the factor  $-1 < \cos(\delta_{R1} - \delta_{R2}) < 1$  and considering the widths of resonances as parameters, the MPCM can reproduce the position and value of the  $S(E)$  minimum. It is important mentioning that at very low energies both factors  $\cos(\delta_{\ ^3S_1(312)} - \delta_{\ ^3S_1(962)})$  and  $\cos(\delta_{R1} - \delta_{R2})$  coincide:  $\cos(\delta_{\ ^3S_1(312)} - \delta_{\ ^3S_1(962)}) \approx \cos(\delta_{R1} - \delta_{R2}) \approx 1$  as seen in Fig. 2. Thus,  $S(0)$  is not sensitive to this factor, while the variation of this factor is important for the description of the value and position of the  $S(E)$  minimum.

The contribution of the  $M1$  non-resonant transition to the GS  $S$ -factor comes out of the MPCM through the  $\ ^3P_1$  scattering state and has significance at the energies  $E_{c.m.} < 500$  keV. This contribution increases with the energy decrease. Consideration of the  $M1$  transition requires the experimental  $(p,p)$  phase shifts. The elastic  $\ ^{15}\text{N}(p,p)\ ^{15}\text{N}$  cross sections are measured only at energies higher than 2.7 MeV [42]. The low energy elastic scattering experimental data are desirable to evaluate the intensity of the  $\ ^3P_1 \longrightarrow \ ^3P_0$   $M1$  transition.

What is the contribution of each transition to the  $S(0)$ ?  $E1(312 \text{ keV})$  provides 15.5 keV·b (41%),  $E1(962 \text{ keV})$  gives 3.9 keV·b (10%),  $M1$  does 2.6 keV·b (7%), and the interference term gives 15.7 keV·b (42%).

$R$ -matrix calculations reproduce the interference minimum. Our consideration of the destructive interference of  $\ ^3S_1(312)$  and  $\ ^3S_1(962)$  resonances did not reproduce the minimum of the  $S$ -factor precisely. The consideration of another state is justified if it has the same quantum numbers  $J^\pi = 1^-$  as the resonances we already considered. Such a state will interfere with the first two  $1^-$  resonances. As was already mentioned in Sec II there is such a resonance in the  $\ ^{16}\text{O}$  spectrum that lays at a very high excitation energy  $E_x = 16.20(90)$  MeV. It is higher than the  $\ ^3S_1(312)$  resonance by 3.76 MeV and by 3.11 MeV higher than the  $\ ^3S_1(962)$ . Our numerical calculations have shown that the effect of this third in the spectrum of  $1^-$  resonances is negligible, and its interference does not influence the value or position of the  $S$ -factor minimum.

In Table 3 the experimental data for the GS astrophysical  $S$ -factor in the measured energy ranges are given. The experimental range of energy is dramatically different which leads to the different values of  $S(E_{\min})$ . In Ref. [13] the cross section is measured for the highest energy. The cross section for the lowest energy  $E_{c.m.} = 70$  keV, which is near of the Gamow range, is reported in Ref. [6]. It is obvious that extrapolation of the  $S(E)$  to the  $S(0)$  using each listed experimental energy range will give the different values of the  $S(0)$ , sometimes dramatically different.

The determination of  $S(0)$  relies on the dual approach of experimental measurement of the cross section complemented by theoretical interpretation and extrapolation from the experimental range of energy to the zero energy. In Table 4 the estimates of the astrophysical  $S$ -factor at zero energy  $S(0)$  obtained using the  $R$ -matrix fits of the different sets of experimental data, different model calculations, and extrapolation of the experimental data are listed. By varying the fitting method, authors obtained different values of  $S(0)$ , see for example Ref. [23]. Theoretical evaluation of astrophysical  $S(E)$  and its extrapolation to  $S(0)$  are also model dependent, consequently, the uncertainties in the computed  $S$ -factor can be significant [65]. The extrapolation is of insufficient accuracy because of the difficulties in taking full account of the complexities of the reaction mechanisms [66] as well.



TABLE 3. Experimental data on the astrophysical  $S$ -factor of the  $^{15}\text{N}(p,\gamma)^{16}\text{O}$  reaction. The values of  $S(E_{\min})$  listed in rows 1 and 2 are taken from Fig. 8 in Ref. [16].

Reference	$E_{c.m.}, \text{keV}$	$E_{\min}, \text{keV}$	$S(E_{\min}), \text{keV}\cdot\text{b}$
	Experimental range		
1 Hebbard et al., 1960 [12]	206 – 656	230	$138.6 \pm 15.2$
2 Brochard et al., 1973 [14]	234 – 1219	256	$215.1 \pm 27.3$
3 Rolfs & Rodney, 1974 [13]	139 – 2344	139	$124.2 \pm 52.6$
4 Bemmerer et al., 2009 [15]	90 – 230	90	$38.4 \pm 5.4$
5 LeBlanc et al., 2010 [16]	123 – 1687	123	$53 \pm 7.1$
6 Caciolli et al., 2011 [6]	70 – 370	70	$52 \pm 4$
7 Imbriani et al., 2012 [17]	131 – 1687	131	$48.4 \pm 4.8$

TABLE 4. Values of the astrophysical  $S(0)$  factor of the  $^{15}\text{N}(p,\gamma)^{16}\text{O}$  reaction. The estimations for values of the  $S(0)$  are obtained based of experimental data from references listed in the parentheses.

Reference	$S(0), \text{keV}\cdot\text{b}$
	32 ([12])
Rolfs & Rodney, 1974 [13]	$64 \pm 6$ ([13])
Barker, 2008 [20]	$\approx 50 - 55$ ([13]) $\approx 35$ ([12])
Mukhamedzhanov et al., 2008 [21]	$36.0 \pm 6$
LeBlanc et al., 2010 [16]	$39.6 \pm 2.6$
Huang et al., 2010 [73]	21.1
Mukhamedzhanov et al., 2011 [23]	33.1 – 40.1
Xu et al., 2013 [19]	$45_{-7}^{+9}$
deBoer et al., 2013 [5]	$40 \pm 3$
Dubovichenko et al., 2014 [22]	39.5 – 43.35
Son et al., 2022 [26]	30.4 ([6])
	$75.3 \pm 12.1$ ([13])
Son et al., 2022 [27]	$34.1 \pm 0.9$ ([16]) $29.8 \pm 1.1$ ([17])
Present work	34.7 – 40.4
Results for $S(0)$ $35.2 \pm 0.5^a$ and $39.6 \pm 0.8^b$ are obtained for AC: $C_w = 1.8^a$ (ANC of $12.85 \text{ fm}^{1/2}$ ) and $C_w = 2.05^b$ (ANC of $14.49 \text{ fm}^{1/2}$ ).	

At ultra-low energies, the energy dependence of the  $S$ -factor can be modified by "a screening effect". The Coulomb screening effects in the laboratory plasma as well as astrophysical environment are discussed in detail in Refs. [67–70]. Despite various theoretical studies conducted over the past two decades, a theory has not yet been found that can explain the cause of the exceedingly high values of the screening potential needed to explain the data [71].

Our expectation is that consideration of the screening will increase  $S(0)$ . The lack of parameters for the screening potential in the  $p^{15}\text{N}$  medium does not allow us to estimate the role of the screening effect in the  $^{15}\text{N}(p,\gamma)^{16}\text{O}$  reaction. However, if one considers the estimation of [72], the enhancement of  $S$ -factor at the energies  $\sim 70 \text{ keV}$  corresponding to the LUNA lower data consists of near 11%.

#### IV. REACTION RATE

The reaction rates for nuclear fusion are the critical component for stellar-burning processes and the study of stellar evolution [4]. In stellar interiors, where the interacting particles follow a Maxwell-Boltzmann distribution, the reaction rate describes the probability of nuclear interaction between two particles with an energy-dependent reaction cross section  $\sigma(E)$ . The reaction rate of proton capture processes can be written as [48, 74].

$$N_A \langle \sigma v \rangle = N_A \left( \frac{8}{\pi \mu} \right)^{1/2} (k_B T)^{-3/2} \int \sigma(E) E \exp\left(-\frac{E}{k_B T}\right) dE = N_A \left( \frac{8}{\pi \mu} \right)^{1/2} (k_B T)^{-3/2} \int S(E) e^{-2\pi\eta} \exp\left(-\frac{E}{k_B T}\right) dE. \quad (6)$$

In Eq. (6)  $N_A$  is the Avogadro number,  $\mu$  is the reduced mass of two interacting particles,  $k_B$  is the Boltzmann constant,  $T$  is the temperature of the stellar environment, and the factor  $e^{-2\pi\eta}$  approximates the permeability of the Coulomb barrier between two point-like charged particles.

### A. $^{15}\text{N}(p,\gamma)^{16}\text{O}$ reaction rate

The reaction rate can be numerically obtained in the framework of the standard formalism outline in Ref. [18] based on the  $S$ -factor that includes the contributions of all transitions shown in Fig. 3 as well as fractional contributions of  $E1$  transitions and  $^3P_1 \rightarrow ^3P_0$   $M1$  transition to the  $^{15}\text{N}(p,\gamma)^{16}\text{O}$  reaction rate. In Fig. 4 the reaction rate and fractional contributions of each transition to the reaction rate are presented. The insert in Fig. 4 shows the contribution of each resonance and  $^3P_1 \rightarrow ^3P_0$  transition with respect to the total reaction rate as a function of astrophysical temperature. Such a presentation is useful to

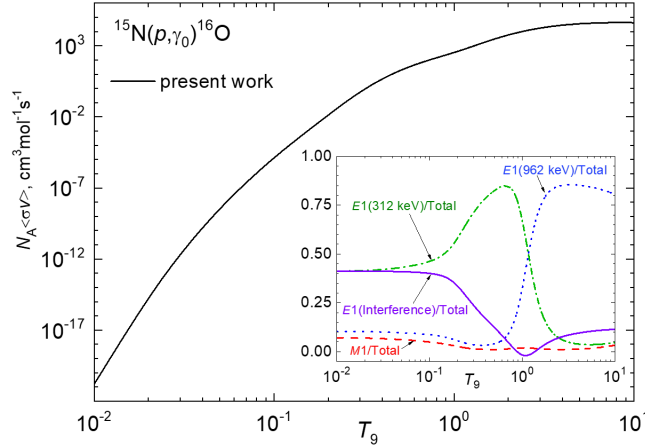


FIG. 4. (Color online) (a) The dependence of the reaction rate of the  $^{15}\text{N}(p,\gamma)^{16}\text{O}$  radiative capture on astrophysical temperature. The solid curve presents our calculations for the sum of  $E1$  and  $M1$  transitions performed for the potentials with the sets of parameters from Table 2. The inset shows the fractional contributions of the reaction rates from the  $^3S_1$  resonances at 312 keV and 962 keV, respectively, and non-resonance transition  $^3P_1 \rightarrow ^3P_0$  with respect to the reaction rate of  $^{15}\text{N}(p,\gamma)^{16}\text{O}$ , as a function of astrophysical temperature.

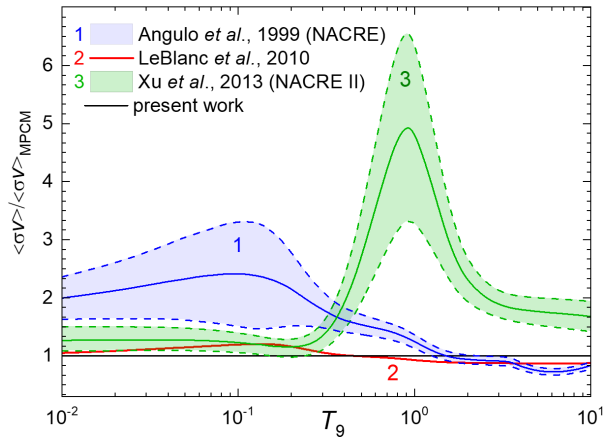


FIG. 5. (Color online) The dependence of the ratio of the proton radiative capture on  $^{15}\text{N}$  reaction rate from NACRE [18] (curve 1), [16] (curve 2), NACRE II [19] (curve 3) and the present calculation on astrophysical temperature in the range of  $T_9 = 0.01 - 10$ . The shaded areas within the dashed curves represent the uncertainties from NACRE and NACRE II. NACRE [18], LeBlanc et al. [16], and present calculations are given for the GS transition and NACRE II parametrization includes the GS transition and transitions via two  $2^-$  resonances, and  $0^-$  and  $3^-$  resonances [19].

understand the relevance of each transition at a given temperature. At  $T_9 = 0.01$  the fractional contribution from the 312 keV resonance is 71%, while the fractional contributions of the 962 keV resonance and non-resonance transition  $^3P_1 \rightarrow ^3P_0$  are

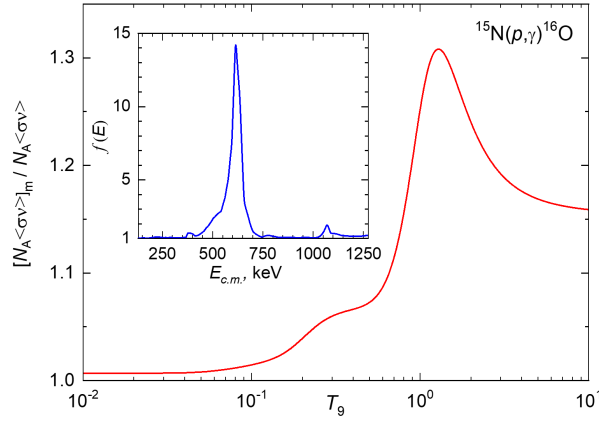


FIG. 6. The dependence of the ratio of the total reaction rate which is the sum of contributions from the  $^{15}\text{N}(p,\gamma_0)^{16}\text{O}$  and cascade transitions  $^{15}\text{N}(p,\gamma_{(6.050)})^{16}\text{O}$ ,  $^{15}\text{N}(p,\gamma_{(6.130)})^{16}\text{O}$ ,  $^{15}\text{N}(p,\gamma_{(7.117)})^{16}\text{O}$  and the reaction rate for the GS transition on temperature. The experimental data reported in Ref. [17] are used in calculations. The inset shows the dependence of the factor  $f(E)$  on the proton energy in the c.m.

16% and 13%, respectively. However, in contrast, at temperature  $T_9 = 10$  the fractional contribution from the 962 keV resonance is 89% and contributions of 312 keV resonance and  $^3P_1 \rightarrow ^3P_0$  transition are commensurate: 6% and 5%, respectively. The E1 transitions from 312 keV and 962 keV resonances have maximal fractional contributions 95% and 93% at  $T_9 = 0.4$  and  $T_9 = 4.1$ , respectively. The fractional contribution from non-resonance transition  $^3P_1 \rightarrow ^3P_0$  increases with the decrease of the energy.

The interference of the  $^3S_1(312)$  and  $^3S_1(962)$  resonances requires special consideration. The solid line in the insert in Fig. 4 shows the fractional contribution of the interference term between the  $^3S_1(312)$  and  $^3S_1(962)$  resonances to the total reaction rate. In the Gamow CNO window  $T_9 = 0.01 - 0.03$  the contribution of the interference term into the total reaction rate is 41% up to  $T_9 = 0.1$ . In the temperature interval  $T_9 = 0.01 - 0.1$  the contribution of the interference term to the total reaction rate is  $\sim 40\%$ , while at  $T_9 = 3 - 10$ , the contribution of this term does not exceed  $\sim 11\%$ . For the stellar CNO temperature range  $T_9 = 0.1 - 0.5$  the contribution of the interference term is dropping from  $\sim 40\%$  to  $\sim 12.5\%$ . The destructive interference is observed in the range from  $T_9 = 0.89$  to  $T_9 = 1.36$ , but on the level of  $\sim 2\%$ . Starting from the end of this interval up to  $T_9 = 10$  a moderate increasing of a constructive interference is observed from zero up to 11%.

The dependence of the reaction rate of the  $^{15}\text{N}(p,\gamma_0)^{16}\text{O}$  radiative capture as a function of temperature for astrophysical temperature between  $T_9 = 0.01$  and  $T_9 = 10$  is shown in Fig. 4. Results for the reaction rates for sets I – III are shown by a single solid curve in Fig. 4. The reaction rates for  $^{15}\text{N}(p,\gamma)^{16}\text{O}$  were reported earlier in Refs. [16, 18, 19]. We normalized the reaction rate obtained within the  $R$ -matrix approach [16], NACRE [18], and NACRE II [19] reaction rates by dividing the corresponding data on the reaction rate obtained in the present calculation. The dependence of these ratios as the function of astrophysical temperature is shown in Fig. 5. One can see the agreement between the reaction rate [16] obtained for the GS transition and our calculation. It should be noted the agreement is also observed for the astrophysical factor: the range of our results for  $S(0)$   $34.7 \leq S(0) \leq 40.4$  keV**·**b and from  $37 \leq S(0) \leq 42.2$  keV**·**b from [16] are overlapping. In calculations of  $S(0)$  in [16] the used ANC of  $23 \pm 3$  fm $^{-1/2}$  is about 3 times larger than the experimental value [21]. One can conclude that the reaction rate is weakly responsive to the value of  $S(0)$ .

One can see the significant discrepancies in the reaction rates, particularly, for NACRE [18] and NACRE II (includes the GS and two  $2^-$ ,  $0^-$  and  $3^-$  resonances) [19] data at temperatures  $T_9 = 0.1$  and  $T_9 = 1$ , respectively, where the ratios reach the maximums. While the difference between [16] and our  $^{15}\text{N}(p,\gamma_0)^{16}\text{O}$  and NACRE II at  $T_9 > 0.3$  is understandable. It is puzzling the significant disagreement in the reaction rates between [16] and our, obtained for the GS transition, comparing to NACRE [18] which also parameterized for the GS transition. Maybe this disagreement is related to the experimental data [12, 13] used for the parametrization of the reaction rate reported in NACRE [18] which were excluded in NACRE II [19] in favor of the post-NACRE data.

The reaction rates reported in [19] include cascade transitions via two  $2^-$  resonances, and  $0^-$  and  $3^-$  of  $^{16}\text{O}$  resonances in the  $0.40 \leq E_R \leq 1.14$  MeV range [17, 34, 36, 64]. It is stated in Ref. [19] the enhancement of the ratio around  $T_9 = 1$  seen in Fig. 5 is owing to the contribution of the cascade transitions, which are not included in NACRE [18]. In Refs. [17, 37] partial cross sections of the radiative proton capture to the GS,  $1^{st}(0^+)$ ,  $2^{nd}(3^-)$ , and  $4^{th}(1^-)$  excited states are measured, and converted to the astrophysical  $S$ -factors of the  $^{15}\text{N}(p,\gamma_0)^{16}\text{O}$ ,  $^{15}\text{N}(p,\gamma_{(6.050)})^{16}\text{O}$ ,  $^{15}\text{N}(p,\gamma_{(6.130)})^{16}\text{O}$ , and  $^{15}\text{N}(p,\gamma_{(7.117)})^{16}\text{O}$  reactions. The experimental data on  $(p,\gamma_1)$ ,  $(p,\gamma_2)$ ,  $(p,\gamma_4)$  were reported by Imbriani *et al.* [37] as cascade transitions. We estimate the contribution of these transitions in the framework of the MPCM based on Imbriani's *et al.* [37] experimental data,

because exact calculations of the cascade transitions are out of the scope of the present paper.

The experimental data [17, 37] for  $S$ -factors listed in the EXFOR database [75] (Hokkaido University Nuclear Reaction Data Centre) were used and interpolated with the Origin Pro 2018 software [76]. The interpolation allows to construct the energy-dependent factor  $f(E) = \frac{\text{Total } S\text{-factor}}{\text{GS } S\text{-factor}}$ , where "Total  $S$ -factor" corresponds to the sum of the  $^{15}\text{N}(p,\gamma_0)^{16}\text{O}$  and the cascade transitions  $^{15}\text{N}(p,\gamma_{(6.050)})^{16}\text{O}$ ,  $^{15}\text{N}(p,\gamma_{(6.130)})^{16}\text{O}$ ,  $^{15}\text{N}(p,\gamma_{(7.117)})^{16}\text{O}$ , and "GS  $S$ -factor" refers to the  $^{15}\text{N}(p,\gamma_0)^{16}\text{O}$ . Introducing this factor into Eq. (6)

$$[N_A \langle \sigma v \rangle]_{\text{m}} = N_A \left( \frac{8}{\pi \mu} \right)^{1/2} (k_B T)^{-3/2} \int S(E) \times f(E) e^{-2\pi\eta} \exp\left(-\frac{E}{k_B T}\right) dE, \quad (7)$$

one can estimate the contribution of the cascade transitions. Thus,  $[N_A \langle \sigma v \rangle]_{\text{m}}$  is a modified GS reaction rate which effectively includes the cascade transitions to the excited states of  $^{16}\text{O}$ :  $^{15}\text{N}(p,\gamma_{(6.050)})^{16}\text{O}$ ,  $^{15}\text{N}(p,\gamma_{(6.130)})^{16}\text{O}$ , and  $^{15}\text{N}(p,\gamma_{(7.117)})^{16}\text{O}$ .

The dependence of factor  $f(E)$  and the ratio of the total experimental  $S$ -factor, that is the sum of the contributions from the GS and the cascade transitions and the reaction rate for the GS transition on the proton energy in the c.m. and astrophysical temperature, respectively, is shown in Fig. 6. The factor  $f(E)$  increases 14 times at  $E_{\text{c.m.}} = 600$  keV. At temperatures above  $T_9 = 0.3$  the cascade gamma-ray transitions to the excited bound states contribute to the total reaction rate. Therefore, the enhancement of the ratio  $[N_A \langle \sigma v \rangle]_{\text{m}} / N_A \langle \sigma v \rangle_{\text{GS}}$  at  $T_9 > 0.3$  is owing to the contribution of the cascade transitions:  $^{15}\text{N}(p,\gamma_{(6.050)})^{16}\text{O}$ ,  $^{15}\text{N}(p,\gamma_{(6.130)})^{16}\text{O}$ , and  $^{15}\text{N}(p,\gamma_{(7.117)})^{16}\text{O}$ . In the temperature range of about  $T_9 = 1 - 1.3$  we have a maximum  $\sim 30\%$  deviation of the total rate from the  $^{15}\text{N}(p,\gamma_0)^{16}\text{O}$  GS transition rate and a deviation  $\sim 15\%$  at  $T_9 = 10$ . Thus, our estimations based on the experimental partial  $S$ -factors contradict to a peculiar enhancement behaviour of the ratio reported in NACRE II at  $0.4 < T_9 < 10$ . The latter calls for a careful theoretical investigation of contributions two interfering resonances  $2^-$  at 12.530 MeV and 12.9686 MeV and two interfering resonances  $3^-$  at 13.142 MeV and 13.265 MeV.

The results of  $R$ -matrix calculations of the reaction rate [16] was parameterized in the form

$$N_A \langle \sigma v \rangle = \frac{a_1 10^9}{T_9^{2/3}} \exp\left[a_2/T_9^{1/3} - (T_9/a_3)^2\right] \left[1.0 + a_4 T_9 + a_5 T_9^2\right] + \frac{a_6 10^3}{T_9^{3/2}} \exp(a_7/T_9) + \frac{a_8 10^6}{T_9^{3/2}} \exp[a_9/T_9] \quad (8)$$

and calculations with the parameters from [16] brought us to  $\chi^2 = 20.8$ . However, by varying the parameters, we get a much smaller  $\chi^2 = 0.4$ . The corresponding parameters are given in the first column in Table 5 in Appendix. Parametrization coefficients of the reaction rate obtained in the framework of MPCM for the analytical expression (8) with the parameters from Table 2 are presented in Appendix and are leading to  $\chi^2 = 0.084$ ,  $\chi^2 = 0.086$ , and  $\chi^2 = 0.09$  for the sets I, II and III, respectively. We also present the parametrization coefficients for  $[N_A \langle \sigma v \rangle]_{\text{m}}$  for the set II.

## B. Comparison of rates for proton capture reactions on nitrogen isotopes

There are two stable nitrogen isotopes  $^{14}\text{N}$  and  $^{15}\text{N}$  and all other radioisotopes are short-lived. Among short-lived isotopes, the longest-lived are  $^{12}\text{N}$  and  $^{13}\text{N}$  with a half-life of about 11 ms and 9.965 min, respectively, and they are of nuclear astrophysics interest. A radiative proton capture on nitrogen isotopes in the reactions  $^{12}\text{N}(p,\gamma)^{13}\text{O}$ ,  $^{13}\text{N}(p,\gamma)^{14}\text{O}$ ,  $^{14}\text{N}(p,\gamma)^{15}\text{O}$ , and  $^{15}\text{N}(p,\gamma)^{16}\text{O}$  produces the short-lived  $^{13}\text{O}$ ,  $^{14}\text{O}$ ,  $^{15}\text{O}$  isotope with a half-life of  $\sim 6$  ms,  $\sim 71$  s and  $\sim 122$  s, respectively, and a stable  $^{16}\text{O}$  nucleus. These radiative capture reactions caused by the electromagnetic interaction are significantly slower than reactions induced by the strong interactions. Therefore, these slow reactions control the rate and time of cycles of oxygen isotopes nucleosynthesis at particular astrophysical temperatures.

The authors of Ref. [77] suggested and discussed three alternative paths of rapid processes of the CNO cycle leading to the formation of  $^{14}\text{O}$  through the breakout reactions  $^9\text{C}(\alpha,p)^{12}\text{N}$  and  $^{11}\text{C}(p,\gamma)^{12}\text{N}$ . These three branches of reaction sequences involve  $^{12}\text{N}(p,\gamma)^{13}\text{O}$ ,  $^{13}\text{N}(p,\gamma)^{14}\text{O}$  processes. Thus, these processes are of particular interest for nuclear astrophysics. In the framework of the MPCM the radiative proton capture on nitrogen isotopes  $^{12}\text{N}$ ,  $^{13}\text{N}$ , and  $^{14}\text{N}$  were investigated [28, 78, 79]. Because the reactions  $^{12}\text{N}(p,\gamma)^{13}\text{O}$ ,  $^{13}\text{N}(p,\gamma)^{14}\text{O}$ , and  $^{14}\text{N}(p,\gamma)^{15}\text{O}$  and the present study of  $^{15}\text{N}(p,\gamma)^{16}\text{O}$  are considered on the same footing within the MPCM, it is useful to compare the reaction rates to understand the relevance of each process at a given astrophysical temperature. We compare the reaction rates for  $^{12}\text{N}(p,\gamma)^{13}\text{O}$ ,  $^{13}\text{N}(p,\gamma)^{14}\text{O}$ ,  $^{14}\text{N}(p,\gamma)^{15}\text{O}$ ,  $^{15}\text{N}(p,\gamma)^{16}\text{O}$  reactions

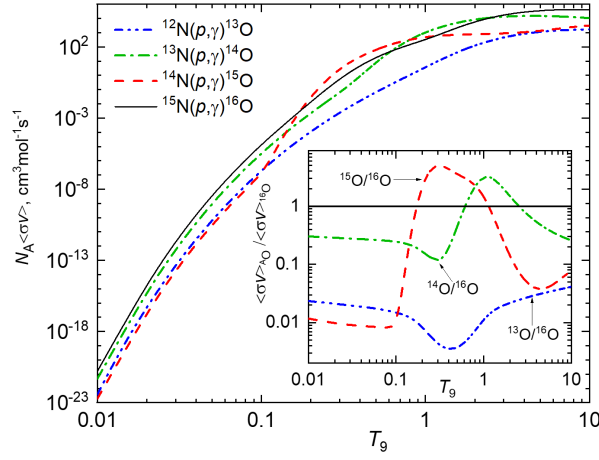
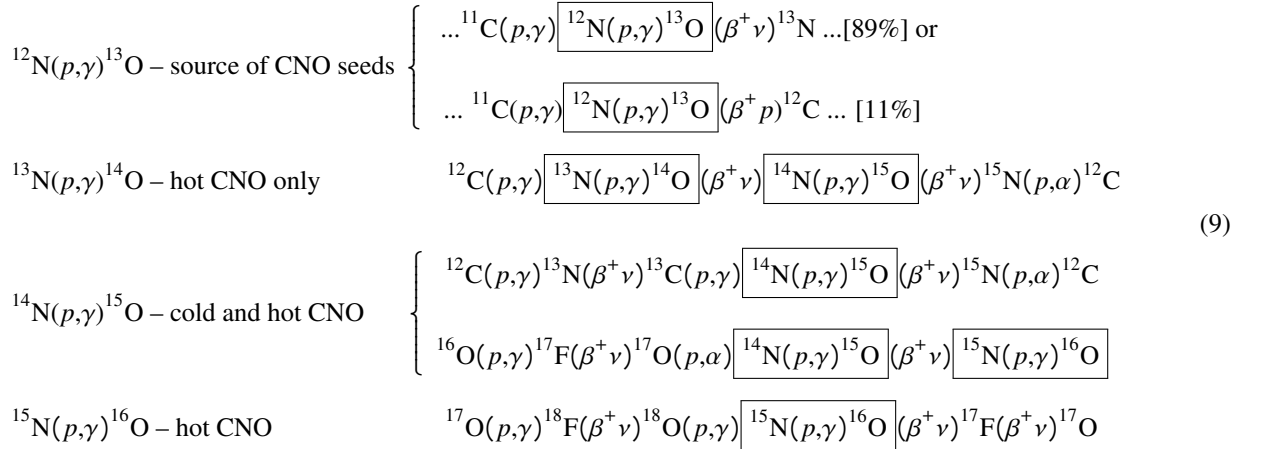


FIG. 7. (Color online) The reaction rates of the radiative proton capture on nitrogen isotopes leading to the production of oxygen isotopes as a function of astrophysical temperature. The insert shows the fractional contributions from  $^{12}\text{N}(p,\gamma)^{13}\text{O}$ ,  $^{13}\text{N}(p,\gamma)^{14}\text{O}$ ,  $^{14}\text{N}(p,\gamma)^{15}\text{O}$  with respect to the  $^{15}\text{N}(p,\gamma)^{16}\text{O}$  reaction rate as a function of astrophysical temperature.

involved into the different chains of the CNO cycles:



The reaction rates of the framed processes are calculated in the framework of the same model, MPCM. The temperature windows, prevalence, and significance of each process are considered. The radiative proton  $^{12}\text{N}(p,\gamma)^{13}\text{O}$ ,  $^{13}\text{N}(p,\gamma)^{14}\text{O}$ ,  $^{14}\text{N}(p,\gamma)^{15}\text{O}$ ,  $^{15}\text{N}(p,\gamma)^{16}\text{O}$  processes have the same Coulomb barrier and, as follows from Eq. (6), the reaction rates will differ only due to the different values of the  $S(E)$  and reduced mass  $\mu$  of interacting particles in the entrance channel. The reduced masses of the pairs  $p^{12}\text{N}$ ,  $p^{13}\text{N}$ ,  $p^{14}\text{N}$ , and  $p^{15}\text{N}$  are always less than the proton mass and are within the range  $0.9294 \text{ amu} \leq \mu \leq 0.9439 \text{ amu}$ . Therefore, the influence of the reduced mass on the reaction rates of the proton capture on nitrogen isotopes is negligible and can be omitted. Therefore, the rates of these processes completely depend on the reaction  $S$ -factor. Figure 7 gives an overview of the reaction rates for typical CNO temperature and explosive hydrogen burning scenarios. The  $^{15}\text{N}(p,\gamma)^{16}\text{O}$  reaction is the fastest one with the biggest rate up to  $T_9 \sim 0.175$  and  $p^{14}\text{N}$  is the slowest process up to  $T_9 \sim 0.1$  and it controls the rate and time of nucleosynthesis cycles. One should notice that  $^{15}\text{N}(p,\gamma)^{16}\text{O}$  rate becomes the dominant one at temperature explosive hydrogen burning scenarios in stars. The analysis of the result presented in the insert in Fig. 7 leads to the conclusion that only in the temperature windows  $0.18 \leq T_9 \leq 1.14$  and  $0.66 \leq T_9 \leq 3$  the reaction  $^{15}\text{N}(p,\gamma)^{16}\text{O}$  is slower than  $^{13}\text{N}(p,\gamma)^{14}\text{O}$  and  $^{14}\text{N}(p,\gamma)^{15}\text{O}$  reactions, respectively. Hence this slow reaction controls the rate and time of cycles of nucleosynthesis.

It is useful to show the reaction rates of proton radiative capture. The radiative hydrogen burning induced nucleosynthesis at specific temperatures has the Gamow peak energy [48, 80]

$$E_0 = \left[ \frac{\pi^2}{\hbar^2} (Z_1 Z_2 e^2)^2 \frac{\mu}{2} (k_B T)^2 \right]^{\frac{1}{3}} \tag{10}$$

which is defined by the condition  $\frac{d}{dE}f_G(E,T) = 0$ , where  $f_G(E,T) = e^{-2\pi\eta} \exp\left(-\frac{E}{k_B T}\right)$  is a Gamow function. In the case of the proton and nitrogen isotopes in the entrance channel  $Z_1 = 1$  and  $Z_2 = 7$  for (10) in keV for temperature  $T_9$  one obtains

$$E_0 = 466.4353 \left[ \mu T_9^2 \right]^{\frac{1}{3}}, \quad (11)$$

and the effective energy range determined by the Gamow range  $\Delta E_G$  (in keV) around the Gamow energy  $E_0$  is

$$\Delta E_G = 452.9821 \left[ \mu T_9^5 \right]^{\frac{1}{6}}. \quad (12)$$

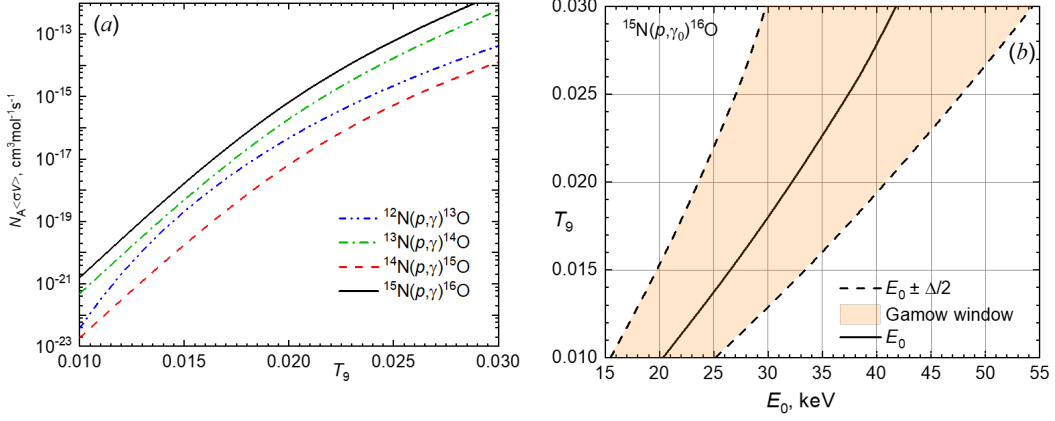


FIG. 8. (Color online) (a) Dependencies of reaction rates of the radiative proton capture on nitrogen isotopes on astrophysical temperature in the range of  $T_9 = 0.01 - 0.03$ . (b) The stellar temperatures as a function of the Gamow energy for CNO cycle  $^{12}\text{N}(p,\gamma)^{13}\text{O}$ ,  $^{13}\text{N}(p,\gamma)^{14}\text{O}$ ,  $^{14}\text{N}(p,\gamma)^{15}\text{O}$  and  $^{15}\text{N}(p,\gamma)^{16}\text{O}$  reactions.

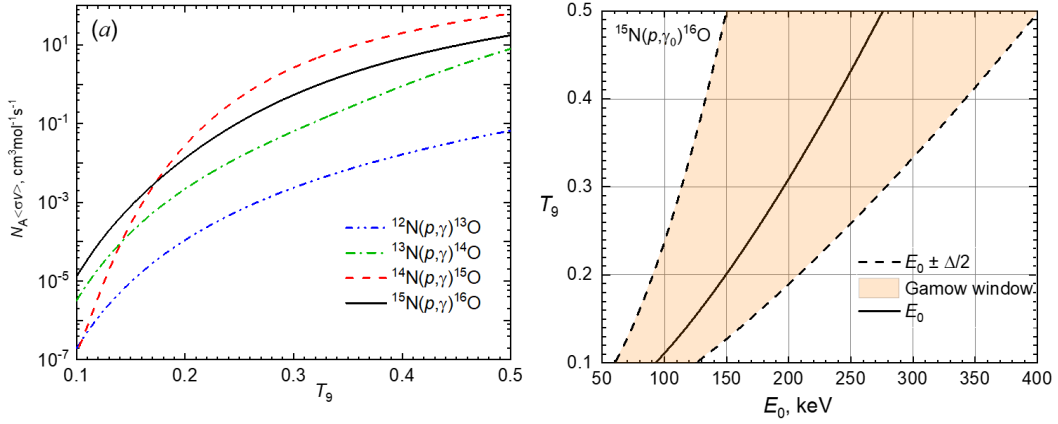


FIG. 9. (Color online) (a) Dependencies of reaction rates of the radiative proton capture on nitrogen isotopes on astrophysical temperature in the range of  $0.1T_9 - 0.5T_9$ . (b) The stellar temperatures as a function of the Gamow energy for CNO cycle  $^{12}\text{N}(p,\gamma)^{13}\text{O}$ ,  $^{13}\text{N}(p,\gamma)^{14}\text{O}$ ,  $^{14}\text{N}(p,\gamma)^{15}\text{O}$  and  $^{15}\text{N}(p,\gamma)^{16}\text{O}$  reactions.

Thermonuclear reactions occur mainly over the Gamow energy window from  $E_0 - \Delta E_G/2$  to  $E_0 + \Delta E_G/2$  except in the case of narrow resonances [48]. From Eqs. (11) and (12) is clear that the Gamow peak energies and ranges for  $^{12}\text{N}(p,\gamma)^{13}\text{O}$ ,  $^{13}\text{N}(p,\gamma)^{14}\text{O}$ ,  $^{14}\text{N}(p,\gamma)^{15}\text{O}$ ,  $^{15}\text{N}(p,\gamma)^{16}\text{O}$  reactions are completely determined by the astrophysical temperature. The variation of the reduced mass within  $0.9294 \text{ amu} \leq \mu \leq 0.9439 \text{ amu}$  changes the Gamow peak energy and the energy range only within 0.5% and 0.3%, respectively.

It is useful to present the reaction rate for a particular temperature range along with the Gamow window of CNO reactions for the radiative proton capture on nitrogen isotopes. The corresponding results of calculations are shown in Figs. 8 and 9. It should be noticed that the main difficulty in determining reliable reaction rates of  $^{12}\text{N}(p,\gamma)^{13}\text{O}$ ,  $^{13}\text{N}(p,\gamma)^{14}\text{O}$ ,  $^{14}\text{N}(p,\gamma)^{15}\text{O}$ ,  $^{15}\text{N}(p,\gamma)^{16}\text{O}$  reactions for the CNO cycles is the uncertainty in the very low cross sections at the Gamow range. Developments within the low-energy underground accelerator facility LUNA in the Gran Sasso laboratory [81] and recent improvements in the detection setup [82] make taking direct measurements of nuclear reactions near the Gamow range feasible. This advantage has been demonstrated in the  $^{14}\text{N}(p,\gamma)^{15}\text{O}$  reaction, which was successfully measured down to energies of 70 keV at LUNA [83].

## V. CONCLUSION

We present the results of calculations and analysis of the astrophysical  $S$ -factor and reaction rate for the  $^{15}\text{N}(p,\gamma)^{16}\text{O}$  reaction in the framework of MPCM with forbidden states, including low-lying  $^3S_1$  resonances and  $^3P_1 \rightarrow ^3P_0$   $M1$  transition. The intercluster potentials of the bound state, constructed on the basis of quite obvious requirements for the description of the binding energy and AC in  $p^{15}\text{N}$  channel of the GS and the scattering potentials describing the resonances, make it possible to reproduce the behavior of available experimental data for the total cross section of radiative proton capture on  $^{15}\text{N}$  nucleus at astrophysical energies. However, it is not so precise as the  $R$ -matrix fitting [5].

The interference of  $^3S_1(312)$  and  $^3S_1(962)$  resonances leads to the significant increase of  $S$ -factor at the energies up to 300 keV. The consideration of interfering  $^3S_1$  resonances and the contribution of  $^3P_1$  scattering wave in  $p + ^{15}\text{N}$  channel due to  $^3P_1 \rightarrow ^3P_0$   $M1$  transition leads to an increase of the  $S$ -factor at low energies. Our result for the  $M1$  transition is related to the corresponding phase shifts. Within our model we demonstrated that the contribution of the  $M1$  transition from the non-resonance  $^3P_1$  scattering wave to the  $^{15}\text{N}(p,\gamma_0)^{16}\text{O}$  cross section really exists and provides  $\sim 7\%$  to the  $S(0)$ . Thus, a systematic and precise low-energy elastic proton scattering data on  $^{15}\text{N}$  are needed to determine phase shifts at the energies  $E_{c.m.} \leq 2$  MeV. The extrapolation of the  $S$ -factor at the low energy leads to  $35.2 \pm 0.5$  keV·b and  $39.6 \pm 0.8$  keV·b, depending on the value of the asymptotic constant, which turned out to be within 34.7 – 40.4 keV·b. It is elucidated the important role of the asymptotic constant for the  $^{15}\text{N}(p,\gamma_0)^{16}\text{O}$  process, where the interfering  $^3S_1(312)$  and  $^3S_1(962)$  resonances give the main contribution to the cross section. A comparison of our calculation for  $S(0)$  with existing experimental and theoretical data shows a reasonable agreement with experimental measurements. Interestingly, the values of  $S(0)$  are consistent with each other, regardless of utilizing various  $R$ -matrix method approaches [5, 16, 19–21, 23] and present MPCM calculations. The deviations of  $S(0)$  in different approaches are within an accuracy of the main sources of uncertainties.

The reaction rate is calculated and parameterized by the analytical expression at temperatures ranging from  $T_9 = 0.01$  to  $T_9 = 10$  and compared with the existing rates. The reaction rate has negligible dependence on the variation of AC, but shows a strong impact of the interference of  $^3S_1(312)$  and  $^3S_1(962)$  resonances, especially at  $T_9$  referring to the CNO Gamow windows. We estimated the contribution of the cascade transitions to the reaction rate. The enhancement of the ratio of the sum of GS and cascade transitions and the GS transition at  $T_9 > 0.3$  is owing to the contribution of the  $^{15}\text{N}(p,\gamma_{(6.050)})^{16}\text{O}$ ,  $^{15}\text{N}(p,\gamma_{(6.130)})^{16}\text{O}$ , and  $^{15}\text{N}(p,\gamma_{(7.117)})^{16}\text{O}$  processes.

**Acknowledgments.** The authors would like to thank A. M. Mukhamedzhanov for useful discussions. This research was supported by the Ministry of Science and Higher Education of the Republic of Kazakhstan under the grant AP09259174.

### Appendix A: Parameters for analytical parameterizations

Parameterization coefficients for the analytical expression (8) of the  $^{15}\text{N}(p,\gamma)^{16}\text{O}$  reaction rate date in Ref. [16] and obtained within the framework of MPCM are presented in Table 5. The sets of parameters I, II, and III from Table 2 lead to the three sets of parametrization coefficients for Eq. (8). The Set II<sub>m</sub> with  $\chi^2 = 0.093$  presents the parametrization coefficients for Eq. (8) when data [37] for the transitions  $^{15}\text{N}(p,\gamma_{(6.050)})^{16}\text{O}$ ,  $^{15}\text{N}(p,\gamma_{(6.130)})^{16}\text{O}$ , and  $^{15}\text{N}(p,\gamma_{(7.117)})^{16}\text{O}$  are considered based on Eq. (7).

- 
- [1] C. A. Barnes, D. D. Clayton, D. N. Schramm, Essays in Nuclear Astrophysics. Presented to William A. Fowler (UK: Cambridge University Press, 1982) p. 562
  - [2] E. G. Adelberger et al., Rev. Mod. Phys., 83: 195 (2011) <https://doi.org/10.1103/RevModPhys.83.195>
  - [3] M. Arnould, S. Goriely, Prog. Part. Nucl. Phys., 112: 103766 (2020) <https://doi.org/10.1016/j.ppnp.2020.103766>
  - [4] M. Wiescher, J. Görres, E. Uberseder, G. Imbriani, M. Pignatari, Annu. Rev. Nucl.Part. Sci., 60: 381 (2010)

TABLE 5. Parameters of analytical parametrization of the reaction rate  $p^{15}\text{N}$  capture. The parameters for the reaction rate presented in Ref. [16] with  $\chi^2 = 0.4$  and results obtained in the present MPCM calculation.

$i$	Parameters for [16]	Parameters for MPCM	Parameters for MPCM		Parameters for MPCM
	$\chi^2 = 0.4$	Set I, $\chi^2 = 0.084$	Set II, $\chi^2 = 0.086$	Set II <sub>m</sub> , $\chi^2 = 0.093$	Set III, $\chi^2 = 0.09$
	$a_i$	$a_i$	$a_i$	$a_i$	$a_i$
1	0.4874952	1.0375	1.00436	0.90521	0.92832
2	-15.22289	-15.41934	-15.4231	-15.39278	-15.42226
3	0.8597972	2.19708	2.17155	2.09762	2.16317
4	6.734083	0.10981	0.10166	0.47779	0.11569
5	-2.462556	-0.01995	-0.01655	-0.04484	-0.01654
6	0.7971639	1.67272	1.72304	1.55827	1.68868
7	-2.930568	-3.0594	-3.06727	-3.03021	-3.07264
8	3.224569	4.38681	4.20809	4.93559	3.97887
9	-11.00680	-12.10183	-12.09517	-12.52017	-12.10662

- [5] R. J. deBoer, J. Görres, G. Imbriani, P. J. LeBlanc, E. Uberseder, M. Wiescher, Phys. Rev. C, 87: 015802 (2013) <https://doi.org/10.1103/PhysRevC.87.015802>
- [6] A. Caciolli, et al., A&A A., 66: 533 (2011) <https://doi.org/10.1051/0004-6361/201117475>
- [7] A. Boeltzig, et al., Eur. Phys. J. A., 52: 75 (2016) <https://doi.org/10.1140/epja/i2016-16075-4>
- [8] G. R. Caughlan, W. A. Fowler, Astrophys. J., 136: 453 (1962) <https://doi.org/10.1086/147399>
- [9] M. J. Harris, W. A. Fowler, G. R. Caughlan, B. A. Zimmerman, Ann. Rev. Astron. Astrophys., 21: 165 (1983). <https://doi.org/10.1146/annurev.aa.21.090183.001121>
- [10] G. R. Caughlan, W. A. Fowler, Atomic Data and Nucl. Data Tables, 40: 283 (1988) [https://doi.org/10.1016/0092-640X\(88\)90009-5](https://doi.org/10.1016/0092-640X(88)90009-5)
- [11] A. Schardt, W. A. Fowler, C. C. Lauritsen, Phys. Rev., 86: 527 (1952) <https://doi.org/10.1103/PhysRev.86.527>
- [12] D. F. Hebbard, Nucl. Phys., 15: 289 (1960) [https://doi.org/10.1016/0029-5582\(60\)90308-4](https://doi.org/10.1016/0029-5582(60)90308-4)
- [13] C. Rolfs, W. S. Rodney, Nucl. Phys. A., 235: 450 (1974) [https://doi.org/10.1016/0375-9474\(74\)90205-X](https://doi.org/10.1016/0375-9474(74)90205-X)
- [14] F. Brochard, P. Chevallier, D. Disdier, F. Scheibling, J. Phys., 34: 363 (1973)
- [15] D. Bemmerer, et al., J. Phys. G: Nucl. Part. Phys., 36: 045202 (2009) <https://doi.org/10.1088/0954-3899/36/4/045202>
- [16] P. J. LeBlanc, et al., Phys. Rev. C., 82: 055804 (2010); Phys. Rev. C., 84: 019902 (2011) <https://doi.org/10.1103/PhysRevC.82.055804>
- [17] G. Imbriani, et al., Phys. Rev. C., 85: 065810 (2012) <https://doi.org/10.1103/PhysRevC.85.065810>
- [18] C. Angulo et al., Nucl. Phys. A., 656: 3 (1999) [https://doi.org/10.1016/S0375-9474\(99\)00030-5](https://doi.org/10.1016/S0375-9474(99)00030-5)
- [19] Y. Xu, et al. Nucl. Phys. A., 918: 61 (2013) <https://doi.org/10.1016/j.nuclphysa.2013.09.007>
- [20] F. C. Barker, Phys. Rev. C., 78: 044612 (2008) <https://doi.org/10.1103/PhysRevC.78.044612>
- [21] A. M. Mukhamedzhanov et al., Phys. Rev. C 78: 015804 (2008) <https://doi.org/10.1103/PhysRevC.78.015804>
- [22] S. B. Dubovichenko, A. V. Dzhazairov-Kakhramanov, Int. J. Mod. Phys. E., 23: 1430012 (2014) <https://doi.org/10.1142/S0218301314300124>
- [23] A. M. Mukhamedzhanov, M. L. Cognata, V. Kroha, Phys. Rev. C., 83: 044604 (2011) <https://doi.org/10.1103/PhysRevC.83.044604>
- [24] X. Z. Li, J. Tian, M. Y. Mei, C. X. Li, Phys. Rev. C., 61: 024610 (2000) <https://doi.org/10.1103/PhysRevC.61.024610>
- [25] S. H. Mondal, Md. A. Khan, Int. J. Mod. Phys. E.:31, 2250045 (2022) <https://doi.org/10.1142/S0218301322500458>
- [26] S. Son, S.-I. Ando, Y. Oh, New Physics: Sae Mulli, 72: 291 (2022)
- [27] S. Son, S.-I. Ando, Y. Oh, Phys. Rev. C., 106: 055807 (2022) <https://doi.org/10.1103/PhysRevC.106.055807>
- [28] S. B. Dubovichenko, R. Ya. Kezerashvili, N. A. Burkova, A. V. Dzhazairov-Kakhramanov, B. Beisenov, Phys. Rev. C., 102: 045805 (2020) <https://doi.org/10.1103/PhysRevC.102.045805>
- [29] S. B. Dubovichenko, A. S. Tkachenko, R. Ya. Kezerashvili, N. A. Burkova, A. V. Dzhazairov-Kakhramanov, Phys. Rev. C., 105: 065806 (2022) <https://doi.org/10.1103/PhysRevC.105.065806>
- [30] S. B. Dubovichenko, Thermonuclear Processes in Stars and Universe. Second English edition, expanded and corrected (Germany: Saarbrücken: Scholar's Press, 2015) p. 332
- [31] S. B. Dubovichenko, Radiative Neutron Capture. Primordial Nucleosynthesis of the Universe (Berlin/Munich/Boston: Walter de Gruyter GmbH., 2019) p. 310
- [32] V. G. Neudatchin, et al., Phys. Rev. C., 45: 1512 (1992) <https://doi.org/10.1103/PhysRevC.45.1512>
- [33] V. I. Kukulin, V. G. Neudatchin, I. T. Obukhovskiy, Yu. F. Smirnov, in *Clustering Phenomena in Nuclei. Clusters as subsystems in light nuclei*. Ed. by K. Wildermuth and P. Kramer, Springer, Brawnschweig, Vol. 3: 4–155 (1983)
- [34] D. R. Tilley, H. R. Weller, C. M. Cheves, Nucl. Phys. A., 564: 1 (1993) [https://doi.org/10.1016/0375-9474\(93\)90073-7](https://doi.org/10.1016/0375-9474(93)90073-7)
- [35] S. I. Sukhoruchkin, Z. N. Soroko, Sub. G. Suppl. I/25 A-F. Springer (2016) <https://doi.org/10.1007/978-3-662-48875-1>
- [36] S. Gorodetzky, J. Adloff, F. Brochard, P. Chevallier, D. Dispier, P. Gorodetzky, R. Modjtahed-Zadeh, F. Scheibling, Nucl. Phys. A., 113: 221 (1968)
- [37] G. Imbriani, et al., Phys. Rev. C., 86: 039902(E) (2012) <https://doi.org/10.1103/PhysRevC.86.039902>
- [38] J. M. Eisenberg, W. Greiner, Nuclear theory. Vol. 2, Excitation mechanisms of the nucleus (Amsterdam: North-Holland Pub. Co., 1976)
- [39] R. J. deBoer, et al., Phys. Rev. C., 85: 038801 (2012) <https://doi.org/10.1103/PhysRevC.85.038801>



- [40] S. Bashkin, R. R. Carlson, R. A. Douglas, *Phys. Rev.*, 114: 1543 (1959) <https://doi.org/10.1103/PhysRev.114.1543>
- [41] R. LaCanna, H. Glavish, J.R. Calarco and S. Hanna, *Bull. Am. Phys. Soc.*, 21: 1294 (1976)
- [42] S. E. Darden, et al., *Nucl. Phys. A.*, 429: 218 (1984) [https://doi.org/10.1016/0375-9474\(84\)90206-9](https://doi.org/10.1016/0375-9474(84)90206-9)
- [43] C. Rolfs, *Nucl. Phys. A.*, 217: 29 (1973) [https://doi.org/10.1016/0375-9474\(73\)90622-2](https://doi.org/10.1016/0375-9474(73)90622-2)
- [44] C. Rolfs, R. E. Azuma, *Nucl. Phys. A.*, 227: 291 (1974) [https://doi.org/10.1016/0375-9474\(74\)90798-2](https://doi.org/10.1016/0375-9474(74)90798-2)
- [45] A. M. Mukhamedzhanov, L. D. Blokhintsev, *Eur. Phys. J. A.*, 58: 29 (2022) <https://doi.org/10.1140/epja/s10050-021-00651-0>
- [46] A. M. Mukhamedzhanov, *Eur. Phys. J. A.*, 59: 43 (2023) <https://doi.org/10.1140/epja/s10050-023-00918-8>
- [47] A. S. Davydov, *Teoriya atomnogo yadra (The theory of the atomic nucleus)* (in Russian) (MOSKVA, 1958) p. 618
- [48] C. Iliadis, *Nuclear Physics of Stars*, 2nd ed., (Weinheim: Wiley-VCH, 2015) p. 672
- [49] F. Ajzenberg-Selove, *Nucl. Phys. A.*, 523: 1 (1991) [https://doi.org/10.1016/0375-9474\(91\)90446-D](https://doi.org/10.1016/0375-9474(91)90446-D)
- [50] J-P Karr, D. Marchand, E. Voutier, *Nature Rev. Phys.*, 2: 601 (2020) <https://doi.org/10.1038/s42254-020-0229-x>
- [51] A. M. Mukhamedzhanov, N. K. Timofeyuk, *Sov. J. Nucl. Phys.*, 51: 431 (1990)
- [52] H. M. Xu, et al., *Phys. Rev. Lett.*, 73: 2027 (1994) <https://doi.org/10.1103/PhysRevLett.73.2027>
- [53] A. M. Mukhamedzhanov, R. E. Tribble, N. K. Timofeyuk, *Phys. Rev. C.*, 51: 3472 (1995) <https://doi.org/10.1103/PhysRevC.51.3472>
- [54] A. M. Mukhamedzhanov, C. A. Gagliardi, R. E. Tribble, *Phys. Rev. C.*, 63: 024612 (2001) <https://doi.org/10.1103/PhysRevC.63.024612>
- [55] N. K. Timofeyuk, R. C. Johnson, A. M. Mukhamedzhanov, *Phys. Rev. Lett.*, 91: 232501 (2003) <https://doi.org/10.1103/PhysRevLett.91.232501>
- [56] A. M. Mukhamedzhanov, et al., *Phys. Rev. C.*, 67: 065804 (2003) <https://doi.org/10.1103/PhysRevC.67.065804>
- [57] N. K. Timofeyuk, *Phys. Rev. Lett.*, 103: 242501 (2009) <https://doi.org/10.1103/PhysRevLett.103.242501>
- [58] N. K. Timofeyuk, *Phys. Rev. C.*, 88: 044315 (2013) <https://doi.org/10.1103/PhysRevC.88.044315>
- [59] R. E. Tribble, C. A. Bertulani, M. La Cognata, A. M. Mukhamedzhanov, C. Spitaleri, *Rep. Prog. Phys.*, 77: 106901 (2014) <https://doi.org/10.1088/0034-4885/77/10/106901>
- [60] L. D. Blokhintsev, D. A. Savin, *Phys. Atom. Nucl.*, 84: 401 (2021) <https://doi.org/10.1134/S1063778821040098>
- [61] G. R. Plattner, R. D. Viollier, *Nucl. Phys. A.*, 365: 8 (1981) [https://doi.org/10.1016/0375-9474\(81\)90384-5](https://doi.org/10.1016/0375-9474(81)90384-5)
- [62] L. D. Blokhintsev, I. Borbey, E. I. Dolinskii, *Phys. Part. Nucl.*, 8: 1189 (1977)
- [63] Centre for photonuclear experiments data, <http://cdfe.sinp.msu.ru>, retrieved 8th February 2015
- [64] F. B. Hagedorn, *Phys. Rev.*, 108: 735 (1957)
- [65] D. G. Yakovlev, M. Beard, L. R. Gasques, M. Wiescher, *Phys. Rev. C.*, 82: 044609 (2010) <https://doi.org/10.1103/PhysRevC.82.044609>
- [66] M. Wiescher, F. Käppeler, K. Langanke, *Annu. Rev. Astron. Astrophys.*, 50: 165 (2012) <https://doi.org/10.1146/annurev-astro-081811-125543>
- [67] C. A. Bertulani, T. Kajino, *Prog. Part. Nucl. Phys.*, 89: 56 (2016) <https://doi.org/10.1016/j.pnpnp.2016.04.001>
- [68] M. Famiano, A. B. Balantekin, T. Kajino, M. Kusakabe, K. Mori, Y. Luo, *Astrophys. J.*, 898: 163 (2020) <https://doi.org/10.3847/1538-4357/aba04d>
- [69] T. Aumann, C. A. Bertulani, *Prog. Part. Nucl. Phys.*, 112: 103753 (2020) <https://doi.org/10.1016/j.pnpnp.2019.103753>
- [70] D. T. Casey, et al., *Front. Phys.*, 10: 1057603 (2023) <https://doi.org/10.3389/fphy.2022.1057603>
- [71] C. Spitaleri, C. A. Bertulani, L. Fortunato, A. Vitturi, *Phys. Lett. B.*, 755: 275 (2016) <https://doi.org/10.1016/j.physletb.2016.02.019>
- [72] H. J. Assenbaum, K. Langanke, C. Rolfs, *Phys. Atomic Nuclei*, 327: 451 (1987)
- [73] T. Huang, C. A. Bertulani, V. Guimarães, *At. Data Nucl. Data Tables*, 96: 824 (2010) <https://doi.org/10.1016/j.adt.2010.06.004>
- [74] M. Wiescher, J. Görres, and H. Schatz, *J. Phys. G: Nucl. Part. Phys.*, 25: R133 (1999)
- [75] Hokkaido University Nuclear Reaction Data Centre (JCPRG), <https://www.jcprg.org/exfor/work/search-963.html>, retrieved 19 November 2022
- [76] OriginLab User Guide, <https://www.originlab.com/doc/Origin-Help/Math-Inter-Extrapolate>, retrieved 11 August 2022
- [77] M. Wiescher, J. Görres, S. Graff, L. Buchmann, and F.-K. Thielemann, *Astrophys. J.*, 343: 352 (1989) <https://doi.org/10.1086/167709>
- [78] S. B. Dubovichenko, N. A. Burkova, D. M. Zazulin, *Nucl. Phys. A.*, 1028: 122543 (2022) <https://doi.org/10.1016/j.nuclphysa.2022.122543>
- [79] S. Dubovichenko, N. Burkova, A. Dzhezairov-Kakhramanov, B. Beysenov, *Int. J. Mod. Phys. E.*, 29: 1930007 (2020) <https://doi.org/10.1142/S0218301319300078>
- [80] W. A. Fowler, G. R. Caughlan, and B. A. Zimmerman, *Annu. Rev. Astron. Astrophys.*, 13: 69 (1975)
- [81] LUNA collaboration: H. Costantini, et al., *Rep. Prog. Phys.*, 72: 086301 (2009) <https://doi.org/10.1088/0034-4885/72/8/086301>
- [82] J. Skowronski, et al., *J. Phys. G: Nucl. Part. Phys.*, 50: 045201 (2023). <https://doi.org/10.1088/1361-6471/acb961>
- [83] LUNA Collaboration: Lemut A, et al., *Phys. Lett. B.*, 634: 483 (2006) <https://doi.org/10.1016/j.physletb.2006.02.021>